ISSN 1949-8470 (online)

World Journal of *Radiology*

World J Radiol 2018 November 28; 10(11): 143-183

Published by Baishideng Publishing Group Inc

WJR World Journal of Radiology

Contents

Monthly Volume 10 Number 11 November 28, 2018

MINIREVIEWS

ORIGINAL ARTICLE

Retrospective Cohort Study

Retrospective Study

Contents

World Journal of Radiology

Volume 10 Number 11 November 28, 2018

ABOUT COVER

Editorial Board Member of *World Journal of Radiology*, Gang-Hua Tang, MD, PhD, Professor, Senior Scientist, Department of Nuclear Medicine, The First Affiliated Hospital, Sun Yat-Sen University, Guangzhou 510080, Guangdong Province, China

AIMS AND SCOPE

World Journal of Radiology (*World J Radiol*, *WJR*, online ISSN 1949-8470, DOI: 10.4329) is a peer-reviewed open access academic journal that aims to guide clinical practice and improve diagnostic and therapeutic skills of clinicians.

WJR covers topics concerning diagnostic radiology, radiation oncology, radiologic physics, neuroradiology, nuclear radiology, pediatric radiology, vascular/interventional radiology, medical imaging achieved by various modalities and related methods analysis. The current columns of *WJR* include editorial, frontier, diagnostic advances, therapeutics advances, field of vision, mini-reviews, review, topic highlight, medical ethics, original articles, case report, clinical case conference (clinicopathological conference), and autobiography.

We encourage authors to submit their manuscripts to *WJR*. We will give priority to manuscripts that are supported by major national and international foundations and those that are of great basic and clinical significance.

INDEXING/ABSTRACTING

World Journal of Radiology is now abstracted and indexed in Emerging Sources Citation Index (Web of Science), PubMed, PubMed Central, China National Knowledge Infrastructure (CNKI), and Superstar Journals Database.

NAME OF JOURNAL
World Journal of Radiology

ISSN
ISSN 1949-8470 (online)

LAUNCH DATE
January 31, 2009

FREQUENCY
Monthly

EDITORS-IN-CHIEF
Neeraj Lalwani, MBBS, MD, Associate Professor

EDITORIAL BOARD MEMBERS
https://www.wjgnet.com/1949-8470/editorialboard.htm

EDITORIAL OFFICE
Jin-Lei Wang, Director

PUBLICATION DATE
November 28, 2018

INSTRUCTIONS TO AUTHORS
https://www.wjgnet.com/bpg/gerinfo/204

GUIDELINES FOR ETHICS DOCUMENTS
https://www.wjgnet.com/bpg/GerInfo/287

GUIDELINES FOR NON-NATIVE SPEAKERS OF ENGLISH
https://www.wjgnet.com/bpg/gerinfo/240

PUBLICATION MISCONDUCT
https://www.wjgnet.com/bpg/gerinfo/208

ARTICLE PROCESSING CHARGE
https://www.wjgnet.com/bpg/gerinfo/242

STEPS FOR SUBMITTING MANUSCRIPTS
https://www.wjgnet.com/bpg/GerInfo/239

ONLINE SUBMISSION
https://www.f6publishing.com

World Journal of Radiology

Submit a Manuscript: https://www.f6publishing.com

World J Radiol 2018 November 28; 10(11): 143-149

DOI: 10.4329/wjr.v10.i11.143

ISSN 1949-8470 (online)

MINIREVIEWS

Review of the role of abdominal imaging in irritable bowel syndrome

Richard G Kavanagh, John O'Grady, Brian W Carey, Owen J O'Connor, Michael M Maher

ORCID number: Richard G Kavanagh (0000-0002-7483-0926); John O'Grady (0000-0002-6704-9277); Brian W Carey (0000-0002-6584-8032); Owen J O'Connor (0000-0002-0276-1335); Michael M Maher (0000-0001-7423-7439).

Author contributions: Kavanagh RG and Maher MM involved with study design, manuscript drafting and revising; O'Grady J and Carey BW involved with manuscript drafting and revising; O'Connor OJ involved with study design, data acquisition, manuscript drafting and revising; all authors given final approval to manuscript publication, and agreed to be accountable for all aspects of the work in ensuring that questions related to the accuracy or integrity of any part of the work are appropriately investigated and resolved.

Conflict-of-interest statement: The authors declare that there is no conflict of interest regarding the publication of this paper.

Manuscript source: Unsolicited

Richard G Kavanagh, Brian W Carey, Owen J O'Connor, Michael M Maher, Department of Radiology, Cork University Hospital, Cork T12 DC4A, Ireland

John O'Grady, Department of Gastroenterology, Cork University Hospital, Cork T12 DC4A, Ireland

John O'Grady, Owen J O'Connor, Michael M Maher, APC Microbiome Ireland, University College Cork, Cork T12 DC4A, Ireland

Abstract

The role of radiologic imaging in the investigation of irritable bowel syndrome (IBS) remains a subject of debate and there is some evidence, from recent studies of utilization of imaging in IBS, which focused on associated costs and radiation exposure, that imaging is being used relatively widely in these patients. This review aims to assess current best evidence to accurately define the role of radiologic imaging in IBS patients. Primary and secondary literature searches were performed. Evidence suggests that the lack of "red flag" or alarm features in IBS patients should reassure the clinician that the diagnosis of IBS is correct and United States and United Kingdom guidelines recommend no radiologic imaging for IBS patients if alarm features are not present. In patients presenting with IBS symptoms and alarm features, radiologic testing may be used to exclude an alternative diagnosis and the imaging modality should be chosen based on the most likely alternative diagnosis.

Key words: Abdominal imaging; Rome criteria; Irritable bowel syndrome

Core tip: Radiologic imaging in irritable bowel syndrome (IBS) remains contentious and the evidence guiding its use is limited. Recent studies indicate that imaging is being widely used in these patients. This review assesses current best evidence for the role of imaging in IBS. Primary and secondary literature searches were performed. The cornerstone of diagnosis remains the Rome criteria. Lack of "red flag" features in IBS patients should strengthen diagnosis of IBS and obviate the need for radiologic imaging. If red flag features are present, appropriate imaging may be used to exclude a suspected alternative diagnosis.

Kavanagh RG, O'Grady J, Carey BW, O'Connor OJ, Maher MM. Review of the role of abdominal imaging in irritable bowel syndrome. *World J Radiol* 2018; 10(11): 143-149
URL: https://www.wjgnet.com/1949-8470/full/v10/i11/143.htm

manuscript

Correspondence to: Brian W Carey, BM BCh, Assistant Lecturer, Department of Radiology, Cork University Hospital, Wilton, Cork T12 DC4A, Ireland.
brian_carey@ucc.ie
Telephone: +353-21-49020288

Received: July 14, 2018
Peer-review started: July 17, 2018
First decision: August 2, 2018
Revised: August 30, 2018
Accepted: October 9, 2018
Article in press: October 9, 2018
Published online: November 28, 2018

DOI: https://dx.doi.org/10.4329/wjr.v10.i11.143

INTRODUCTION

Irritable bowel syndrome (IBS) is a chronic functional gastrointestinal disorder (FGID) that is broadly characterized by recurrent abdominal pain and alterations in stool consistency or form[1]. Multinational expert groups in FGIDs have devised the Rome criteria, most recently Rome IV criteria, as a symptom-based diagnostic standard to diagnose IBS. Despite this, as IBS is associated with loss of work days and productivity and negatively impacts quality of life, it often remains a diagnosis of exclusion after invasive investigations are performed to rule out other specific pathology. Interestingly, a comparison of an exclusion approach to diagnosis of IBS, using investigations such as sigmoidoscopy, and a positive diagnostic approach using the Rome criteria, showed little differences in terms of patients' health-related quality of life in one Danish study of over 300 patients[2]. The positive diagnostic approach based on Rome criteria, was however, cheaper when compared to the exclusion approach. This study supports current guideline recommendations and suggests an unnecessary reliance on alternative diagnostic investigations.

Epidemiology

The worldwide prevalence of IBS is estimated to be 7%-10% with wide geographic variability[3]. In the United States the prevalence of IBS is estimated to be approximately 10% to 15%[4] and one large European prospective, population-based cohort study estimated prevalence of 15.4%[5]. IBS is less common in people older than 50 compared with those younger than 50 (OR 0.75)[6] and is more common in women compared with men (OR 1.67)[7]. IBS may be associated with a number of other disorders including fibromyalgia, depression, chronic fatigue syndrome, non-cardiac chest pain and anxiety[4]. There is conflicting evidence regarding IBS prevalence and socioeconomic status[6,8,9] and this relationship remains unproven.

Pathophysiology

That the diagnosis and management of IBS relies on clinical symptoms highlights that the pathophysiology remains incompletely understood. Initial research in the early 20th century utilizing direct visualization of the gastric mucosa in patients with gastrocutaneous fistulae provided the first scientific evidence that the gut is physiologically responsive to stressful emotional and environmental stimuli. Later studies showed that patients with IBS-type symptoms had an enhanced gastrointestinal motor response to various stimuli such as fatty meals, peptide hormones and psychological stressors and increased motility was sometimes associated with pain[10]. Recent advances in knowledge have, however, facilitated an increased understanding of the underlying disease processes, but it remains likely that there are multiple etiological factors involved. Those currently implicated in IBS symptom presentation include altered gastrointestinal motility, visceral hypersensitivity, post-infectious gastroenteritis, intestinal inflammation, altered gut microbiota, food sensitivity and interactions of the brain-gut axis[11]. IBS linked to brain-gut interactions is suggested by the association of IBS with anxiety, depression and other psychiatric conditions[1]. Furthermore, it is recognized that psychological stress exacerbates and exaggerates the symptoms of IBS and associated psychological and psychiatric co-morbidity negatively influence the patient experience of the condition[12]. Persistent post infectious gastroenteritis IBS-type symptoms are common in up to 20% of cases[1], and this is linked to an intestinal inflammatory etiology indicating an alternate pathogenesis to brain-gut interactions[13]. Further etiological factors for IBS development include alterations in gut microbiota and associated predisposing influences on both the microbiome and IBS symptoms including host genetics, stress, diet, antibiotic use and early life experiences[14]. Gut microbiota and their metabolites have notable influences on recognised IBS associations including the brain-gut axis, visceral hypersensitivity, gastrointestinal motility, intestinal barrier function and immune regulation[14]. Though causation is not established, the expanding science of the human gut microbiome and microbe-host interactions suggest gut microbial alterations play a key role in IBS pathophysiology[14]. These various pathophysiological factors may co-exist in the same patient, adding to the heterogeneity and complexity of understanding IBS and may, in part, explain the varying response to current symptom based treatments[15].

Diagnosis

The Rome criteria are criteria that were devised by expert consensus for the diagnosis of FGIDs; these criteria define multiple different FGID including IBS. The most recent iteration of these criteria is the Rome IV, released in 2016. The diagnostic criteria for IBS by the Rome IV criteria are as follows[16]: Recurrent abdominal pain, on average, at least one day per week in the last 3 mo associated with two or more of the following: Pain related to defecation; Associated with a change in frequency of stool; Associated with a change in form (appearance) of stool. The criteria should be fulfilled for the last 3 mo with symptom onset at least 6 mo before diagnosis.

By the Rome IV criteria, the IBS subtype is classified based on the predominant symptom of constipation or diarrhea as follows[16]: IBS with predominant constipation (IBS-C); IBS with predominant diarrhea (IBS-D); IBS with mixed bowel habits (IBS-M); IBS unclassified (IBS-U).

This classification is based upon the percentage of different stool types as defined by the Bristol stool scale. IBS-C is diagnosed if > 25% are stool type 1 and 2 and < 25% are stool type 6 and 7; IBS-D is diagnosed if < 25% are stool type 1 and 2 and > 25% are stool type 6 and 7; and IBS-M is diagnosed if > 25% are stool type 1 and 2 and > 25% are stool type 6 and 7. IBS-U is diagnosed if the patient meets diagnostic criteria for IBS but stool type cannot be accurately categorized into one of the other subtypes.

Assessment for alarm features should be performed in all patients that meet the diagnostic criteria for IBS[17]. The aim of identifying alarm features is to allow consideration of further investigations in patients with signs/symptoms of other possible underlying conditions such as colorectal/ovarian cancer and inflammatory bowel disease. Alarm features include the following[16,18,19]: New onset, or overt, rectal bleeding or melena; Nocturnal pain or diarrhea; Iron-deficiency anemia; Unexplained weight loss; Family history of colon cancer, ovarian cancer, celiac disease, IBD; Fever; Age of onset > 50 years; Severe or progressively worsening symptoms; Abdominal/pelvic/rectal mass or lymphadenopathy; Recent change in bowel habits.

Although the prevalence of alarm features is high in IBS patients[18] the sensitivity of alarm features in predicting organic disease in patients with typical symptoms of IBS is low. This may be due to the fact that besides celiac disease, which a large systematic review demonstrated is four times as prevalent in patients with IBS compared with the general population[20], the prevalence of underlying organic disease is the same in patients with IBS as in the general population[3]. However, certain alarm features such as weight loss and anemia do offer high specificity for organic disease and the American College of Gastroenterology (ACG) state that the absence of alarm features should reassure the clinician that the diagnosis of IBS is correct[3].

IBS burden of disease

IBS is a disease that is associated with significantly reduced health-related quality of life and impaired work productivity[3]. IBS patients utilize 50% more healthcare resources than matched controls without IBS and overall direct and indirect annual healthcare costs in these patients are estimated at $20 billion[3]. This increased cost can be attributed not only to increased medication use but also increased diagnostic testing and lost wages. In 1995, Talley *et al*[21] estimated the excess yearly direct healthcare cost of IBS in the United States to be $8 billion and extrapolating from that study, excess cost of approximately $800 million was estimated for radiology services in these patients. This highlights the importance of accurately defining the role of radiologic imaging in the investigation of patients presenting with IBS-type symptoms in order to rationalize the use of this expensive and, in certain jurisdictions, limited resource.

As well as increased costs, another concern regarding the over-utilization of radiologic diagnostic testing is the radiation exposure imparted as a result of plain radiography, nuclear medicine and CT imaging. Although there is evidence of significant costs associated with radiologic imaging in these patients there is a paucity of studies assessing radiation exposure in this patient group. Englund *et al*[22] demonstrated that over a 10-year period in Sweden, 149 IBS patients had a radiation exposure similar to that of a subgroup of patients with ulcerative colitis. A direct comparison of radiation exposure in IBS patients with that of the general population was not performed in this study so it is difficult to draw conclusions from these results. This result does, however, again demonstrate that radiologic imaging is still being used frequently in the investigation of patients with IBS.

ROLE OF RADIOLOGIC IMAGING IN IBS

The exact role of abdominal radiologic imaging in IBS remains poorly defined and

some studies suggest that imaging is being used relatively widely in this patient population[21,22]. There is a marked paucity of modern scientific studies regarding the appropriate use of imaging in this patient group[23].

In terms of international guidelines, the ACG state the following in their position statement on IBS[3] based on an evidence-based systematic review[24]: "Routine diagnostic testing with complete blood count, serum chemistries, thyroid function studies, stool for ova and parasites, and abdominal imaging is not recommended in patients with typical IBS symptoms and no alarm features because of a low likelihood of uncovering organic disease".

The ACG do recommend serological testing for celiac disease and colonoscopy in patients with alarm features and those over the age of 50 to assess for colorectal cancer. When colonoscopy is performed in patients with IBS-D, the ACG recommend random biopsies are taken to assess for microscopic colitis.

The United Kingdom National Institute for Health and Care Excellence (NICE) guidelines address the use of radiologic testing explicitly in their recommendations as follows[17]: "The following tests are not necessary to confirm diagnosis in people who meet the IBS diagnostic criteria: Ultrasound; Rigid/flexible sigmoidoscopy; Colonoscopy; barium enema; Thyroid function test; Faecal ova and parasite test; Faecal occult blood; Hydrogen breath test".

In an evidence-based review of the role of abdominal radiologic imaging in IBS by O'Connor *et al*[23] in 2012, the authors assessed that the best available evidence that included seven systematic reviews/guidelines and five primary research articles focusing on the use of barium enema and/or ultrasound. The authors concluded that radiologic imaging is not required in patients fulfilling the clinical diagnostic criteria for IBS if alarm symptoms are not present. The authors also concluded that further investigation should be considered in patients with alarm features and the appropriate modality should be chosen on a case-by-case basis and guided by the most likely alternative diagnosis and the American College of Radiology (ACR) Appropriateness Criteria. The lack of robust evidence and prospective studies regarding the role of abdominal radiologic imaging is noted in this review.

Since this review, several studies have used MRI to investigate IBS patients. These studies aimed to demonstrate differences in bowel response to food ingestion in IBS patients relative to healthy volunteers[25,26] and differences between the various IBS subtypes[27]. These studies suggest various sites of pathology to explain IBS symptoms but it is difficult to draw any firm conclusions from these studies due to small numbers and heterogeneous, and sometimes conflicting, results. No definitive role has been established for the routine use of MRI in the investigation of IBS and no studies have been performed to assess the performance of MRI relative to symptom-based diagnostic criteria.

In the setting of IBS patients that also demonstrate alarm features, further investigations should be guided by the most likely alternative diagnosis; this will often involve endoscopic assessment of the bowel but radiologic testing has a role in some circumstances. For example if a patient presents with signs/symptoms suggestive of colorectal cancer NICE guidelines recommend direct visualization with colonoscopy/sigmoidoscopy or CT colonography in patients unfit for colonoscopy. In the setting of a suspected ovarian neoplasm a pelvic ultrasound is the first investigation recommended by the ACR. In a patient with signs/symptoms suggestive of inflammatory bowel disease radiologic imaging studies (*e.g.*, CT or MR enterography) may be used to supplement findings on laboratory and endoscopic studies in order to establish a diagnosis[28].

CONCLUSION

There remains a paucity of robust evidence regarding the appropriate use of abdominal radiologic imaging in the setting of IBS and no modern prospective studies exist. Symptom-based diagnostic criteria have a high sensitivity and specificity for diagnosing IBS. Alarm symptoms are common in IBS patients but demonstrate low sensitivity for alternative organic pathology if diagnostic criteria for IBS are satisfied. Weight loss and anemia have a high specificity for underlying organic disease and in patients meeting diagnostic criteria without alarm features, clinicians should be reassured that the diagnosis of IBS is correct.

Based on the current best evidence, the diagnosis of IBS should be based on clinical findings using expert consensus diagnostic criteria (Rome IV criteria) supplemented by laboratory testing with no role for abdominal radiologic imaging in most patients. In patients presenting with IBS symptoms and alarm features, radiologic testing may be used to investigate for an underlying organic disease and the imaging modality

should be chosen based on the most likely alternative diagnosis (see Table 1 for practice guideline recommendations).

Table 1 Practice guideline recommendations

Patients fulfilling the Rome IV diagnostic criteria for IBS and who do not display "red flag" symptoms such as blood in stool, weight loss, recurrent fevers, anemia, and chronic severe diarrhea and who have no family history of colorectal cancer, inflammatory bowel disease, or celiac sprue do not require radiologic imaging
Radiologic imaging is required in patients with "red flag" symptoms who fulfill the Rome IV diagnostic criteria for IBS
Consideration of the probable alternative diagnosis and adherence to the relevant American College of Radiology Appropriateness Criteria should direct the optimal radiologic imaging of the patient with IBS

IBS: Irritable bowel syndrome.

REFERENCES

1 **Ford AC**, Lacy BE, Talley NJ. Irritable Bowel Syndrome. *N Engl J Med* 2017; **376**: 2566-2578 [PMID: 28657875 DOI: 10.1056/NEJMra1607547]
2 **Begtrup LM**, Engsbro AL, Kjeldsen J, Larsen PV, Schaffalitzky de Muckadell O, Bytzer P, Jarbøl DE. A positive diagnostic strategy is noninferior to a strategy of exclusion for patients with irritable bowel syndrome. *Clin Gastroenterol Hepatol* 2013; **11**: 956-62.e1 [PMID: 23357491 DOI: 10.1016/j.cgh.2012.12.038]
3 **American College of Gastroenterology Task Force on Irritable Bowel Syndrome**, Brandt LJ, Chey WD, Foxx-Orenstein AE, Schiller LR, Schoenfeld PS, Spiegel BM, Talley NJ, Quigley EM. An evidence-based position statement on the management of irritable bowel syndrome. *Am J Gastroenterol* 2009; **104** Suppl 1: S1-35 [PMID: 19521341 DOI: 10.1038/ajg.2008.122]
4 **Wald A**. Clinical manifestations and diagnosis of irritable bowel syndrome in adults. 2014; Available from: https://www.uptodate.com/contents/clinical-manifestations-and-diagnosis-of-irritable-bowel-syndrome-in-adults
5 **Krogsgaard LR**, Engsbro AL, Jones MP, Bytzer P. The epidemiology of irritable bowel syndrome: Symptom development over a 3-year period in Denmark. A prospective, population-based cohort study. *Neurogastroenterol Motil* 2017; 29 [PMID: 27865035 DOI: 10.1111/nmo.12986]
6 **Lovell RM**, Ford AC. Global prevalence of and risk factors for irritable bowel syndrome: a meta-analysis. *Clin Gastroenterol Hepatol* 2012; **10**: 712-721.e4 [PMID: 22426087 DOI: 10.1016/j.cgh.2012.02.029]
7 **Lovell RM**, Ford AC. Effect of gender on prevalence of irritable bowel syndrome in the community: systematic review and meta-analysis. *Am J Gastroenterol* 2012; **107**: 991-1000 [PMID: 22613905 DOI: 10.1038/ajg.2012.131]
8 **Zhu JZ**, Yan TL, Yu CH, Wan XY, Wang YM, Li YM. Is national socioeconomic status related to prevalence of irritable bowel syndrome? *J Gastroenterol Hepatol* 2014; **29**: 1595-1602 [PMID: 24888296 DOI: 10.1111/jgh.12609]
9 **Rey E**, Talley NJ. Irritable bowel syndrome: novel views on the epidemiology and potential risk factors. *Dig Liver Dis* 2009; **41**: 772-780 [PMID: 19665952 DOI: 10.1016/j.dld.2009.07.005]
10 **Drossman DA**. Functional Gastrointestinal Disorders: History, Pathophysiology, Clinical Features and Rome IV. *Gastroenterology* 2016; **pii**: S0016-5085(16)00223-7 [PMID: 27144617 DOI: 10.1053/j.gastro.2016.02.032]
11 **Occhipinti K**, Smith JW. Irritable bowel syndrome: a review and update. *Clin Colon Rectal Surg* 2012; **25**: 46-52 [PMID: 23449495 DOI: 10.1055/s-0032-1301759]
12 **Vanner S**, Greenwood-Van Meerveld B, Mawe G, Shea-Donohue T, Verdu EF, Wood J, Grundy D. Fundamentals of Neurogastroenterology: Basic Science. *Gastroenterology* 2016; **pii**: S0016-5085(16)00184-0 [PMID: 27144618 DOI: 10.1053/j.gastro.2016.02.018]
13 **Keely S**, Walker MM, Marks E, Talley NJ. Immune dysregulation in the functional gastrointestinal disorders. *Eur J Clin Invest* 2015; **45**: 1350-1359 [PMID: 26444549 DOI: 10.1111/eci.12548]
14 **Bhattarai Y**, Muniz Pedrogo DA, Kashyap PC. Irritable bowel syndrome: a gut microbiota-related disorder? *Am J Physiol Gastrointest Liver Physiol* 2017; **312**: G52-G62 [PMID: 27881403 DOI: 10.1152/ajpgi.00338.2016]
15 **Tanaka Y**, Kanazawa M, Fukudo S, Drossman DA. Biopsychosocial model of irritable bowel syndrome. *J Neurogastroenterol Motil* 2011; **17**: 131-139 [PMID: 21602989 DOI: 10.5056/jnm.2011.17.2.131]
16 **Mearin F**, Lacy BE, Chang L, Chey WD, Lembo AJ, Simren M, Spiller R. Bowel Disorders. *Gastroenterology* 2016; **pii**: S0016-5085(16)00222-5 [PMID: 27144627 DOI: 10.1053/j.gastro.2016.02.031]
17 National Institute for Clinical Excellence. Irritable bowel syndrome in adults: diagnosis and management. NICE guidelines [CG61] 2008. Available from: https://www.nice.org.uk/guidance/cg61/chapter/1-recommendations
18 **Black TP**, Manolakis CS, Di Palma JA. "Red flag" evaluation yield in irritable bowel syndrome. *J Gastrointestin Liver Dis* 2012; **21**: 153-156 [PMID: 22720303]
19 **Chey WD**, Kurlander J, Eswaran S. Irritable bowel syndrome: a clinical review. *JAMA* 2015; **313**: 949-958 [PMID: 25734736 DOI: 10.1001/jama.2015.0954]
20 **Ford AC**, Chey WD, Talley NJ, Malhotra A, Spiegel BM, Moayyedi P. Yield of diagnostic tests for celiac disease in individuals with symptoms suggestive of irritable bowel syndrome: systematic review and meta-analysis. *Arch Intern Med* 2009; **169**: 651-658 [PMID: 19364994 DOI: 10.1001/archinternmed.2009.22]
21 **Talley NJ**, Gabriel SE, Harmsen WS, Zinsmeister AR, Evans RW. Medical costs in community subjects with irritable bowel syndrome. *Gastroenterology* 1995; **109**: 1736-1741 [PMID: 7498636 DOI: 10.1016/0016-5085(95)90738-6]
22 **Englund H**, Lidén K K, Lind T, Sundström T, Karling P. Radiation exposure in patients with inflammatory bowel disease and irritable bowel syndrome in the years 2001-2011. *Scand J*

Gastroenterol 2017; **52**: 300-305 [PMID: 27832710 DOI: 10.1080/00365521.2016.1252945]
23 **O'Connor OJ**, McSweeney SE, McWilliams S, O'Neill S, Shanahan F, Quigley EM, Maher MM. Role of radiologic imaging in irritable bowel syndrome: evidence-based review. *Radiology* 2012; **262**: 485-494 [PMID: 22156992 DOI: 10.1148/radiol.11110423]
24 **Rosenblatt WH**, Cioffi AM, Sinatra R, Saberski LR, Silverman DG. Metoclopramide: an analgesic adjunct to patient-controlled analgesia. *Anesth Analg* 1991; **73**: 553-555 [PMID: 1952134]
25 **Undseth R**, Berstad A, Kløw NE, Arnljot K, Moi KS, Valeur J. Abnormal accumulation of intestinal fluid following ingestion of an unabsorbable carbohydrate in patients with irritable bowel syndrome: an MRI study. *Neurogastroenterol Motil* 2014; **26**: 1686-1693 [PMID: 25271767 DOI: 10.1111/nmo.12449]
26 **Pritchard SE**, Marciani L, Garsed KC, Hoad CL, Thongborisute W, Roberts E, Gowland PA, Spiller RC. Fasting and postprandial volumes of the undisturbed colon: normal values and changes in diarrhea-predominant irritable bowel syndrome measured using serial MRI. *Neurogastroenterol Motil* 2014; **26**: 124-130 [PMID: 24131490 DOI: 10.1111/nmo.12243]
27 **Lam C**, Chaddock G, Marciani Laurea L, Costigan C, Cox E, Hoad C, Pritchard S, Gowland P, Spiller R. Distinct Abnormalities of Small Bowel and Regional Colonic Volumes in Subtypes of Irritable Bowel Syndrome Revealed by MRI. *Am J Gastroenterol* 2017; **112**: 346-355 [PMID: 27958282 DOI: 10.1038/ajg.2016.538]
28 **Peppercorn MA**, Kane SV. Clinical manifestations, diagnosis and prognosis of Crohn disease in adults. 2014; Available from: https://www.uptodate.com/contents/zh-Hans/clinical-manifestations-diagnosis-and-prognosis-of-crohn-disease-in-adults

P- Reviewer: Mahajan A, Plataniotis G, Valek V
S- Editor: Ji FF **L- Editor:** A **E- Editor:** Huang Y

World Journal of Radiology

Submit a Manuscript: https://www.f6publishing.com

World J Radiol 2018 November 28; 10(11): 150-161

DOI: 10.4329/wjr.v10.i11.150

ISSN 1949-8470 (online)

ORIGINAL ARTICLE

Retrospective Cohort Study

Significance of an additional unenhanced scan in computed tomography angiography of patients with suspected acute aortic syndrome

Nikolaos Panagiotopoulos, Felix Drüschler, Martin Simon, Florian M Vogt, Sebastian Wolfrum, Steffen Desch, Doreen Richardt, Jörg Barkhausen, Peter Hunold

ORCID number: Nikolaos Panagiotopoulos (0000-0002-3029-9360); Felix Drüschler (0000-0001-9616-8665); Martin Simon (0000-0003-4187-4663); Florian M Vogt (0000-0002-3720-4010); Sebastian Wolfrum (0000-0001-6941-0030); Steffen Desch (0000-0002-9416-8044); Doreen Richardt (0000-0003-1398-8671); Jörg Barkhausen (0000-0001-8937-1198); Peter Hunold (0000-0003-4416-5934).

Author contributions: Hunold P, Vogt FM, Drüschler F designed research; Vogt FM, Drüschler F, Simon M, Hunold P acquired data; Panagiotopoulos N, Vogt FM, Drüschler F, Hunold P analyzed data; Panagiotopoulos N, Hunold P wrote the paper; Barkhausen J, Drüschler F, Simon M, Vogt FM, Wolfrum S, Desch S, Richardt D, Barkhausen J revised and approved final manuscript version

Institutional review board statement: The institutional review board of the University of Lübeck approved this study. This retrospective cohort study and all procedures performed involving human participants were in accordance with the ethical standards of the institutional review board and with the 1964 Helsinki declaration and its later amendments or comparable ethical standards.

Nikolaos Panagiotopoulos, Jörg Barkhausen, Peter Hunold, Clinic for Radiology and Nuclear Medicine, University Hospital Schleswig-Holstein, Campus Lübeck, Lübeck 23538, Germany

Felix Drüschler, Department of Nephrology, University Hospital, Heidelberg 69120, Germany

Martin Simon, Radiologische Allianz, Hamburg 20259, Germany

Florian M Vogt, Radiologie München, München 80331, Germany

Sebastian Wolfrum, Interdisciplinary Emergency Department, University Hospital Schleswig-Holstein, Campus Lübeck, Lübeck 23538, Germany

Steffen Desch, Department of Cardiology, Leipzig University, Heart Centre Leipzig, Leipzig 04289, Germany

Doreen Richardt, Department of Cardiac and Thoracic Vascular Surgery, University Hospital Schleswig-Holstein, Campus Lübeck, Lübeck 23538, Germany

Abstract

AIM

To assess potential benefits of an additional unenhanced acquisition in computed tomography angiography (CTA) in patients with suspected acute aortic syndrome (AAS).

METHODS

A total of 103 aortic CTA (non-electrocardiography-gated, 128 slices) performed due to suspected AAS were retrospectively evaluated for acute aortic dissection (AAD), intramural hematoma (IMH), or penetrating aortic ulcer (PAU). Spiral CTA protocol consisted of an unenhanced acquisition and an arterial phase. If AAS was detected, a venous phase (delay, 90 s) was added. Images were evaluated for the presence and extent of AAD, IMH, PAU, and related complications. The diagnostic benefit of the unenhanced acquisition was evaluated concerning detection of IMH.

RESULTS

Fifty-six (30% women; mean age, 67 years; median, 68 years) of the screened individuals had AAD or IMH. A triphasic CT scan was conducted in 76.8% (n = 43). 56% of the detected AAD were classified as Stanford type A, 44% as Stanford

Conflict-of-interest statement: None of the authors states a conflict of interest concerning firms and products reported in this study.

Data sharing statement: No additional data are available.

Manuscript source: Invited manuscript

Correspondence to: Peter Hunold, MD, Assistant Professor, Vice Chairman, Clinic for Radiology and Nuclear Medicine, University Hospital Schleswig-Holstein, Campus Lübeck, Ratzeburger Allee 160, Lübeck 23538, Germany. peterhunold@icloud.com
Telephone: +49-451-50017010
Fax: +49-451-50017004

Received: April 30, 2018
Peer-review started: April 30, 2018
First decision: June 14, 2018
Revised: August 30, 2018
Accepted: October 9, 2018
Article in press: October 9, 2018
Published online: November 28, 2018

type B. 53.8% of the detected IMH were classified as Stanford type A, 46.2% as Stanford type B. There was no significant difference in the involvement of the ascending aorta between AAD and IMH (P = 1.0) or in the average age between AAD and IMH (P = 0.548), between Stanford type A and Stanford type B in general (P = 0.650) and between Stanford type A and Stanford type B within the entities of AAD and IMH (AAD: P = 0.785; IMH: P = 0.146). Only the unenhanced acquisitions showed a significant density difference between the adjacent lumen and the IMH (P = 0.035). Subadventitial hematoma involving the pulmonary trunk was present in 5 patients (16%) with Stanford A AAD. The difference between the median radiation exposure of a triphasic (2737 mGy*cm) compared to a biphasic CT scan (2135 mGy*cm) was not significant (P = 0.135).

CONCLUSION
IMH is a common and difficult to detect entity of AAS. An additional unenhanced acquisition within an aortic CTA protocol facilitates the detection of IMH.

Key words: Aortic dissection; Acute aortic syndrome; Intramural hematoma; Pulmonary trunk subadventitial hematoma; Computed tomography angiography

Core tip: A computed tomography protocol in patients with suspected acute aortic syndrome should routinely include an unenhanced acquisition due to the added value in the detection of intramural hematoma.

Panagiotopoulos N, Drüschler F, Simon M, Vogt FM, Wolfrum S, Desch S, Richardt D, Barkhausen J, Hunold P. Significance of an additional unenhanced scan in computed tomography angiography of patients with suspected acute aortic syndrome. *World J Radiol* 2018; 10(11): 150-161
URL: https://www.wjgnet.com/1949-8470/full/v10/i11/150.htm
DOI: https://dx.doi.org/10.4329/wjr.v10.i11.150

INTRODUCTION

Acute aortic syndrome (AAS) is a life threatening condition that subsumes acute aortic dissection (AAD), intramural hematoma (IMH), and penetrating aortic ulcer (PAU)[1]. In-hospital mortality can be as high as 68% within the first 2 d after admission[2]. Recent advances in medical imaging and treatment have further emphasized the importance of rapid and accurate assessment of suspected AAS. In this emergency setting, computed tomography angiography (CTA) is today's benchmark modality[3]. Although detection of an IMH might profoundly influence therapeutic decision-making compared to classic AAD, it is often missed in CT scans of patients with AAS. Thus changes to the routinely performed biphasic CTA protocol with an arterial and a venous acquisition seem necessary. The aim of this study was therefore to assess the potential benefit of a CTA protocol that includes an additional unenhanced acquisition added to contrast-enhanced scans in the diagnostic pathway of patients with AAS. The focus was on the impact on the detectability of IMH in particular. Moreover, we aimed at working out the morphological characteristics of the different entities of AAS (*i.e.*, AAD, IMH, and PAU) as well as the prevalence of related complications (*e.g.*, aortic root subadventitial hematoma and branch vessel involvement).

MATERIALS AND METHODS

Study population

This retrospective cohort study was performed after approval by the institutional review board. CTA examinations of patients with clinically suspected AAS, who had been referred by the emergency department for aortic CTA, were screened. In the surveyed period of 33 mo, 103 aortic CTA scans had been conducted for the indication

of AAS in our radiological department.

Scan protocol

Scans were acquired at a 128-slice CT scanner (Somatom Definition AS+, Siemens Healthcare, Erlangen, Germany). No electrocardiography (ECG)-gating was used. Iodinated contrast agent (IMERON 300, Bracco Imaging, Milan, Italy) was applied by a contrast media injector (ohio tandem, Ulrich medical, Ulm, Germany) injecting 100 mL at a flow of 5 mL/s over an antecubital vein *via* a 18G cannula. We used a potentially triphasic CT protocol consisting of first an unenhanced spiral acquisition of the entire aorta. Secondly, an arterial CTA of the entire aorta was performed. Bolus timing was done using "care bolus" technique with the region of interest (ROI) within the ascending aorta with a threshold of 120 Hounsfield units (HU). If AAS was detected in the arterial phase, a venous phase scan was performed with a delay of 90 s after injection start. The scanning volume of all acquisitions reached from the aortic arch down to the groin.

Image analysis

CT images were digitally reviewed in a Picture archiving and communication system (PACS; IMPAX EE, Agfa HealthCare GmbH, Bonn). To visually delineate and locate AAD, IMH, PAU, and related complications predefined morphological criteria were applied. AAD was identified by findings like an intimal flap and a double lumen in the contrast-enhanced scans[4,5]. If present, the extent of dissection was determined and the Stanford classification system[6] was used according to involvement of the ascending aorta. Moreover, the true lumen of an AAD was distinguished from the false lumen by characteristic features as outer wall calcifications, differences in the caliber of the lumina, the beak sign or the cobweb sign. An essential part of the assessment of the false lumen was to identify a possible partial or total thrombosis by measuring the radiodensity of both lumina in predefined slices in the following regions of the aorta: (1) ascending aorta at the level of the main pulmonary artery; (2) aortic arch; (3) descending aorta at the level of the main pulmonary artery; (4) abdominal aorta at the level of the superior mesenteric artery origin; and (5) abdominal aorta above the bifurcation.

In AAD, radiodensity of both lumina in all acquired phases was measured by placing and adjusting a ROI into the true and false lumen respectively. The radiodensity was recorded as the mean value for each region and phase in HU. In a second step, the discrepancy in density between the true and false lumen was calculated for each region and phase, separately.

Likewise, morphological criteria were applied to identify an IMH. These lesions feature a crescentic, high-attenuating (60-70 HU) region of thickening of the aortic wall on non-contrast CT. The lesions apparently exhibit no enhancement in relation to the aortic lumen on contrast-enhanced scans. An intimal flap is not present. Analogously to AAD, the Stanford classification system was used to classify IMH. Its radiodensity was measured and the discrepancy in density between the wall hematoma and the aortic lumen was calculated and processed for each region and phase separately. The extent or amount of complications related to AAD or IMH like dissections and occlusions of branch vessels, ischemia of abdominal organs, aneurysmal dilatation, aortic rupture, and aortic root subadventitial hematoma were studied in this work as well. The ten evaluated branch vessels were: (1) brachiocephalic trunk; (2) left common carotid artery; (3) left subclavian artery; (4) celiac trunk; (5) superior mesenteric artery; (6) inferior mesenteric artery; (7) renal arteries, left and right; and (8) common iliac arteries, left and right.

For every scan the radiation exposure was measured by the CT dose-length product (DLP; in mGy*cm) which was found in the corresponding DICOM-Header. Gender and age of the study patients was stored and processed.

Statistical analysis

All data were first collected on standardized and anonymized data collection sheets and later transferred into an Excel-file (Microsoft Corporation, Redmond, United States) and SPSS (IBM, Armonk, United States) for statistical analysis. Prior to the comparison of continuous variables in different groups, chi-square test was used to confirm or rule out normal distribution. Since all of the tested groups revealed non-Gaussian distribution, the non-parametric Mann-Whitney *U* test was used to evaluate differences. $P < 0.05$ was considered to indicate statistical significance.

RESULTS

Study cohort

One-hundred-three patients had been diagnosed with aortic dissection or IMH. After the exclusion of those individuals who had chronic aortic dissection (n = 9) or a history of aortic surgery (n = 38) the resulting study cohort consisted of 56 individuals with first diagnosis of AAS (19 women; mean age 66.6 years, range 35-88 years, Figure 1 and Table 1). Among all patients diagnosed with AAS, 76.8% of patients were diagnosed with AAD compared to 23.2% with IMH. PAU was not found in our cohort. There was no significant percentage-difference of Stanford classification between AAD and IMH (P = 1). Age between AAD and IMH patients (P = 0.548) as well as between Stanford A and B (P = 0.650) patients did not differ significantly (Table 1).

Radiation dose

Radiation exposure as well as the share the unenhanced acquisition adds to the examination is depicted in Table 2. There was a higher mean radiation exposure of triphasic (2737.2 mGy*cm) compared to biphasic CT scans (2134.6 mGy*cm).

Characterization of dissection and IMH

Extent and boundaries: Two data sets were excluded as the distal boundary of the AAD/IMH was not within the scan volume. In 31.5%, AAD and IMH were limited to the thoracic aorta. In contrast to IMH, which never involved the iliac arteries, AAD extended into the iliac arteries in 36.6% (Figure 2). Anatomic features such as kinking of the aorta, aortic bifurcation or aneurysm detained a distal progression of AAD and IMH in 41.5% and 53.8%, respectively (P = 0.528, Figure 3).

True and false lumen: In Stanford A AAD, in 95.8% the false lumen was located in the dextrolateral quadrant of the ascending aorta. Stanford A IMH was most frequently found in the sinistrolateral quadrant (57.1%). In the aortic arch, the false lumen and IMH mainly involved the anterior, caudal and posterior quadrant, less frequently they involved the ostia of the supraaortic branches. In Stanford A AAD, the false lumen of the descending thoracic and suprarenal abdominal aorta was predominantly present in the sinistrolateral and dorsal quadrant. In Stanford B AAD, there was only a slight predominance for the dorsal and dextrolateral quadrant. At the level of the renal arteries the false lumen was more often found on the right than the left side (right: Stanford A: 73.9%; Stanford B: 52.6%; left: A: 30.4%; B: 42.1%). In the infrarenal portion of the aorta, there was no significant difference in the position of the false lumen between Stanford A and B (dextroposterior). In the descending thoracic and abdominal aorta, IMH showed no predominance of location.

Involvement of branch vessels: Six data sets were excluded as an assessment of all ten predefined branch vessels was not possible. Branch vessel involvement was only 38.5% in IMH compared to 75.7% in AAD (P = 0.012). In 46% at least two branch vessels and in 20% at least four branch vessels were involved. In 34% there was no branch vessel and in one case (2%) seven branch vessels affected. In AAD there were a total of 225 branch vessels involved (A: 137; B: 88). 131 vessels originated from the true lumen [A: 69 (50.4%); B: 62 (70.5%)], 34 vessels from the false lumen [A: 27 (19.7%); B: 7 (8.0%)], and 60 vessels were supplied by both lumina [A: 41 (29.9%); B: 19 (21.6%)]. Branches that were supplied by the false lumen were patent in 23 cases [A: 19 (70.4%); B: 4 (57.1%)], partly thrombosed in 7 cases [A: 6 (22.2%); B: 1 (14.3%)] and occluded in 4 cases [A: 2 (7.4%); B: 2 (28.6%)]. Branches that were supplied by both the true and the false lumen were patent in 45 cases [A: 30 (73.2%); B: 15 (78.9%)], partly thrombosed in 6 cases [A: 5 (12.2%); B: 1 (5.3%)] and occluded in 9 cases [A: 6 (14.6%); B: 3 (15.8%)]. The brachiocephalic trunk was the vessel most often involved (57.2%). In Stanford A dissections involvement of the coeliac trunk and the superior mesenteric artery was more commonly seen than in Stanford B dissections (A: 38.5%, B: 26.7%; A: 41.7%, B: 13.3%; respectively). By tendency, renal artery involvement was more often present at the left side (A: 63.7%, B: 35.7%) compared to the right side (A: 36.4%, B: 28.6%), (P = 0.424).

Density measurements

In the arterial phase the radiodensity of the patent false lumen of the thoracic aorta was comparable to that of the true lumen, while in the abdominal aorta the radiodensity in the patent false lumen was lower (on average more than 100 HU difference) than in the true lumen (Figure 4 and Figure 5). In the unenhanced and venous acquisitions 241 the radiodensity of the patent false lumen was comparable to that of the true lumen. A false lumen thrombosis resulted in higher radiodensity in the false lumen for the unenhanced acquisitions and lower densities in the arterial and venous phases. IMH had a lower radiodensity compared to the vessel lumen within the arterial and venous phases. In the unenhanced acquisition the radiodensity of the

Table 1 Stanford classification, age and gender distribution

	AAD			IMH		
n (%)	43 (76.8)			13 (23.2)		
mean age (yr)	66 ± 12			69 ± 10		
	Stanford A	Stanford B	A *vs* B	Stanford A	Stanford B	A *vs* B
	55.8%	44.2%		53.8%	46.2%	
mean age (yr)	66 ± 11	67 ± 13	$P = 0.785$	65 ± 10	75 ± 13	$P = 0.146$
Female	41.7%	10.5%	$P = 0.039$	28.6%	50%	

There is no significant difference in the age distribution between Stanford A and B within the entities of acute aortic dissection (AAD) and intramural hematoma. Though, in AAD there is a significant difference in the gender distribution between Stanford A and B dissections. Females showed a significantly higher percentage of type A than type B AAD. AAD: Acute aortic dissection; IMH: Intramural hematoma.

IMH was higher than the adjacent lumen in any of the regions of the aorta in which it occurred (Figure 6). Differences in radiodensity between true lumen and IMH as well as true lumen and thrombosed false lumen, respectively, were only significant in the unenhanced acquisition ($P = 0.035$).

Complications and secondary findings

Table 3 summarizes complications and secondary findings. Subadventitial hematoma involving the pulmonary trunk was present exclusively in patients with Stanford A lesions. It was found in 5 patients, *i.e*. in 16.1% of Stanford A lesions. In these patients pericardial effusion was present in 80%. In two cases there was pulmonary hemorrhage present. The subadventitial hematoma was hypodense in contrast enhanced scans compared to the lumen of the vessel (average HU differences arterial: 436 HU, venous 109 HU) while in non-contrast scans it was hyperdense (average HU difference -13 HU).

Pericardial effusion was significantly more frequent in Stanford A lesions ($P = 0.011$). There was no significant difference in the occurrence of pleural effusion/hemothorax between Stanford A and B ($P = 0.357$). Abdominal aortic aneurysm was more frequent in Stanford B dissections (66.7%). Bleeding or rupture occurred in four Stanford B cases. Although less frequent in IMH, branch vessel involvement was the most frequent complication with 66% in total. Ischemia of abdominal organs was found in 18.2% with kidneys being the most often affected (12.5%).

DISCUSSION

When contemplating the assumption that a multiphasic CTA protocol adding a non-enhanced acquisition significantly improves the detectability of AAD and IMH there is the dimension of fast and accurate visualization and that of radiation protection that has to be evaluated. In this respect, this study shows that the radiodensity of the true lumen and the false lumen of AAD do not differ significantly in contrast-enhanced scans. On the contrary, unenhanced acquisitions featured a high-attenuating region of thickening of the aortic wall with a significant density difference between the IMH and the adjacent lumen in the range of 5 HU up to 21 HU for all examined regions of the aorta. A differentiation between IMH and a thrombosed false lumen was possible due to the significantly higher contrast between IMH and adjacent lumen compared to thrombotic material and adjacent lumen ($P = 0.035$). While the mere figures might seem rather small, the reason for the resulting critical improvement in the visualisation of the potentially life-threatening entity IMH can be found in the way windowing is possible if no contrast agent is used. By lowering the window level and narrowing the window width, the interpreting physician is able to zero in on those aspects that are of diagnostic value. While the arterial phase is essential for the delineation of pathognomonic findings like an intimal flap and a double lumen[7] and the venous acquisitions facilitate the assessment of the patency of the false lumen as well as a possible ischemia of the abdominal organs, adding an unenhanced acquisition of the thoracic aorta should be used whenever an AAS is suspected. In this study we were able to identify 13 IMH and 5 aortic root subadventitial hematomas and to distinguish both these entities from a false lumen thrombosis. This would not have been possible without the data of the unenhanced scan. The diagnosis of an IMH might profoundly influence the therapeutic decision-

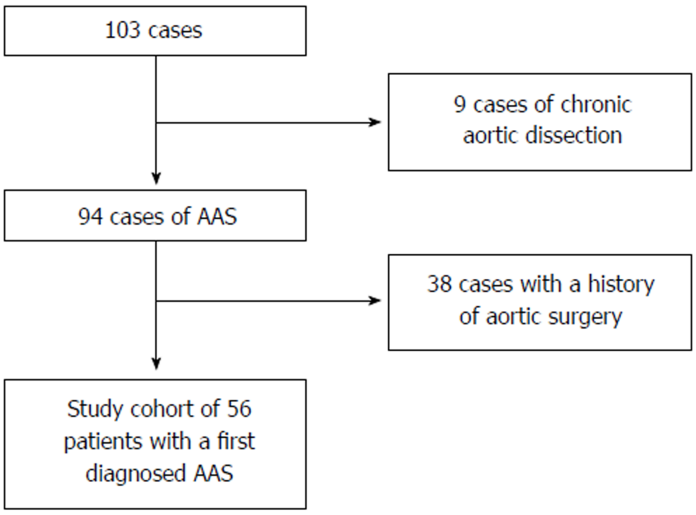

Figure 1 Selection process of the study cohort. After the exclusion of chronic dissections and patients with a history of aortic surgery, 56 cases made up the study cohort of individuals with a newly diagnosed acute aortic syndrome. AAS: Acute aortic syndrome.

making compared to classic aortic dissection. First of all, IMH has a higher rate of rupture as compared to AAD[8]. Research groups around the world have argued about the right treatment of IMH. According to Tsai *et al*[9], similar to Stanford type A and B aortic dissection, surgery is advocated in patients with Stanford type A IMH and initial medical therapy in patients with type B IMH. On the contrary, a study conducted by Song *et al*[10] showed acceptable outcomes of a policy of urgent surgery for unstable Stanford type A IMH patients and initial medical treatment for stable patients with surgery for complications. In 2014 the European Society of Cardiology issued a guideline[11]. In accordance with this guideline, "emergency surgery of IMH is indicated in complicated cases with pericardial effusion (in this study present in type A: 71.4%, B: 0%), periaortic hematoma (in this study present in: type A: 42.9%, B: 0.0%), or large aneurysms [in this study present in (AAA): type A: 0.0%, B: 50.0%]. Surgery within 24 h after diagnosis is required in most of Stanford type A IMH. In elderly patients or those with significant comorbidities, initial medical treatment may be a reasonable option. Medical treatment is the initial approach to Stanford type B IMH. Endovascular therapy or surgery has the same indications as type B aortic dissection. While there might still be debate about the treatment that is clinically indicated if an IMH is detected, the importance of a rapid and accurate detection and assessment of potentially life-threatening complications is out of doubt. Nonetheless the ALARA principle ("as low as reasonably achievable") dictates a limitation of the patients' radiation exposure. Our data indicate that adding an unenhanced acquisition to a biphasic CT scan does, as expected, increase the radiation exposure, but to a moderate degree of only 22% to the total radiation dose. Therefore the risk of overlooking an IMH or aortic root subadventitial hematomata seems to be grossly disproportionate to the benefit of a reduction in radiation exposure. In our opinion the added radiation dose of a triphasic protocol is reasonable and can easily be justified. The data of this study substantiate the common perception that an IMH is a more circumscript thoracic pathology that rarely affects the abdominal aorta. This finding allowed us to further adjust our CTA protocol and operating procedures in a way that reduces the patients' radiation exposure while maintaining most of the benefits the unenhanced acquisition offers. In cases in which there is no clinical suspicion of an abdominal involvement we now limit the unenhanced scan to the thoracic aorta, lowering the radiation exposure.

The 56 cases diagnosed with AAS would translate into an incidence of about 8.9/100000 a year if the population of Lübeck[12] is regarded as the hinterland of our department of radiology and nuclear medicine. This figure is considerably higher than the 2.9/100000/year incidence found in literature[2].

Studies based on the International Registry of Acute Aortic Dissections have found about 6.3% of AAS to be IMH[13]. In our cohort the prevalence was as high as 23.2%. This discrepancy partly originates from the study design and the selection process of the study cohort which excluded about 46% of patients with AAS because of a chronic aortic dissection or a history of aortic surgery. As many IMH evolve into an AAD

Table 2 Radiation exposure as measured by the computed tomography dose-length product

	DLP [mGy*cm]		
	Mean	Min	Max
Triphasic CT scan (unenhanced, arterial and venous)	2737.2	1583.0	4476.9
Biphasic CT scan (arterial and venous)	2134.6	766.2	3494.7
Unenhanced acquisition (percentage of a triphasic CT scan)	602.6 (22.0%)		

Adding an unenhanced acquisition to a biphasic computed tomography (CT) scan does, as expected, increase radiation exposure, however to a moderate degree. On average the unenhanced acquisition contributes only about 22% to the total radiation dose of a triphasic CT scan. DLP: Dose-length product.

there might be a selection bias due to the small study cohort as well. However, one might also suggest that IMH has often been overseen if the utilized CTA protocol misses a focus on detection of even small IMH. Therefore, adding an unenhanced scan to the CTA is suggested.

Limitations

Although the screened cohort of 868 individuals was sizable, the resulting study cohort on which our data is based (n = 56) is not. The small size of this retrospective cohort study limits the generalizability of the results. A further limitation of this work can be found in the definition of branch vessel involvement. A branch vessel involvement was defined as an intimal flap or a hematoma that extended into the branch or alternatively the sole perfusion by false lumen. This definition leaves out any type of dynamic obstruction. Nonetheless, we believe that this study offers some motivational thoughts and descriptions of clinical relevance.

Table 3 Complications and secondary findings *n* (%)

	Total	AAD		IMH	
		Stanford A	Stanford B	Stanford A	Stanford B
Subadventitial hematoma of pulmonary trunk	5 (9.1)	2 (8.3)	0	3 (42.9)	0
Pericardial effusion	20 (35.7)	11 (45.8)	4 (21.1)	5 (71.4)	0
Pleural effusion	14 (25.0)	4 (16.7)	6 (31.6)	2 (28.6)	2 (33.3)
Abdominal aortic aneurysm (AAA)	17 (32.1)	2 (8.7)	12 (66.7)	0	3 (50.0)
Bleeding/rupture	4 (7.1)	0	3 (15.8)	0	1 (16.7)
Branch vessel involvement	33 (66.0)	17 (81.0)	12 (70.6)	3 (50.0)	1 (16.7)
Ischemia	10 (18.2)	5 (20.8)	4 (22.2)	1 (14.3)	0
Kidney	7 (12.5)	4 (16.7)	3 (15.8)	0	0
Liver	2 (3.6)	1 (4.2)	1 (5.3)	0	0
Spleen	3 (5.5)	0	2 (11.1)	1 (14.3)	0
Intestine	1 (1.8)	0	1 (5.3)	0	0

Branch vessel involvement was the most frequent complication. Subadventitial hematoma involving the pulmonary trunk was present exclusively in patients with Stanford A lesions. Pericardial effusion was significantly more frequent in Stanford A lesions. AAD: Acute aortic dissection; IMH: Intramural hematoma.

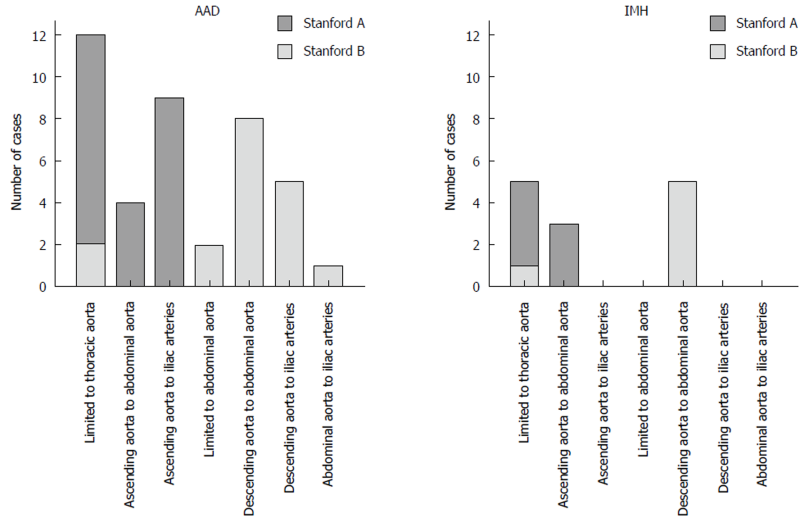

Figure 2 Extent of dissection and intramural hematoma. Nearly one third of acute aortic syndrome was limited to the thoracic aorta. There was no case in which the intramural hematoma extended into the iliac arteries. AAD: Acute aortic dissection; IMH: Intramural hematoma.

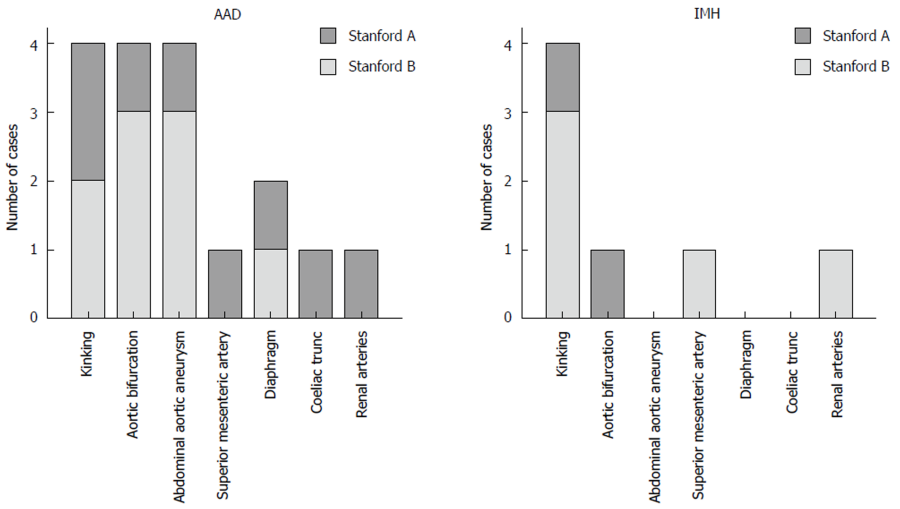

Figure 3 Boundaries of acute aortic dissection and intramural hematoma. Anatomic features detain a distal progression of acute aortic dissection and intramural hematoma. AAD: Acute aortic dissection; IMH: Intramural hematoma.

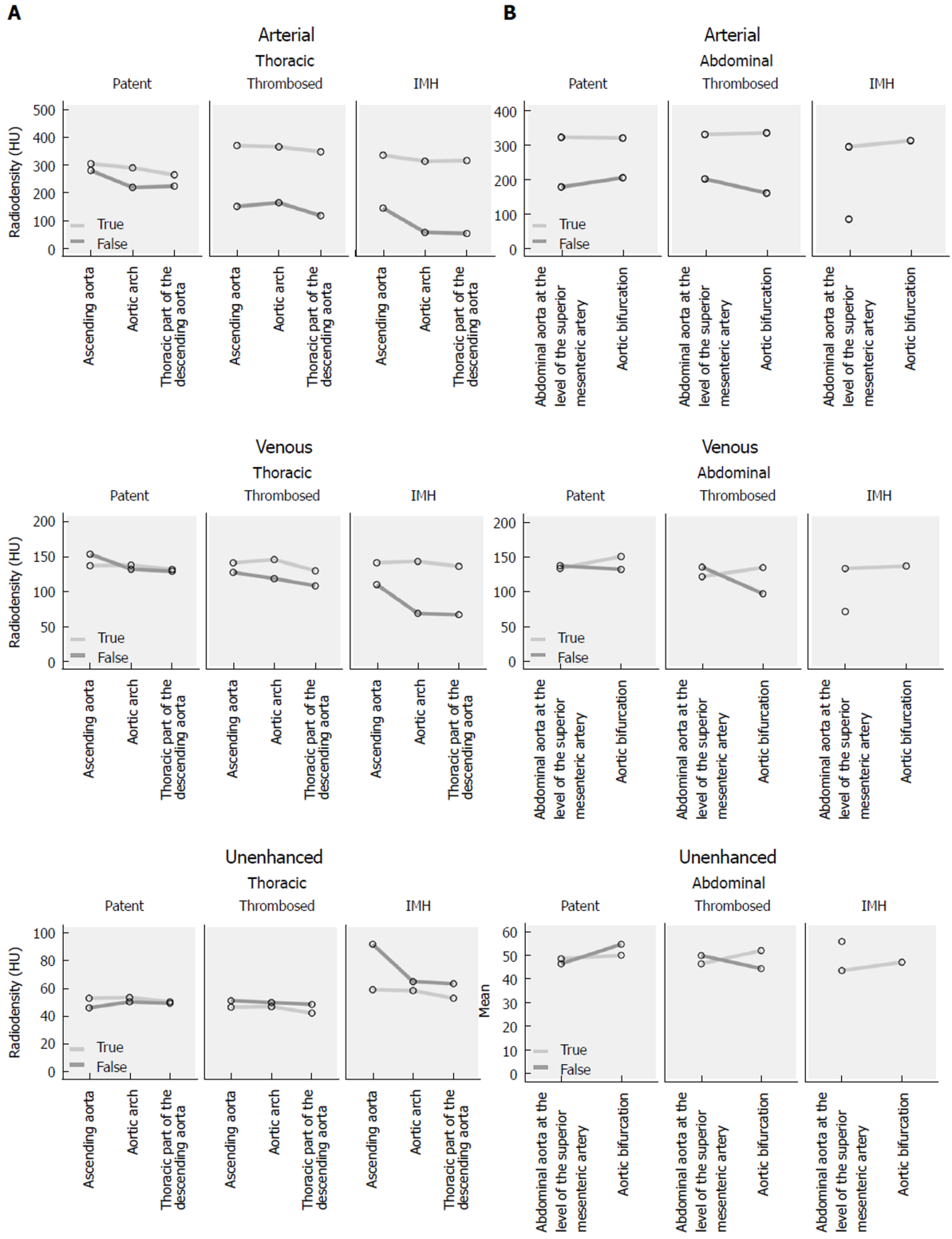

Figure 4 Density measurements, absolute values. Absolute values of the density measurements in true and false lumen/intramural hematoma in arterial, venous and unenhanced phase of (A) thoracic and (B) abdominal aorta. IMH: Intramural hematoma.

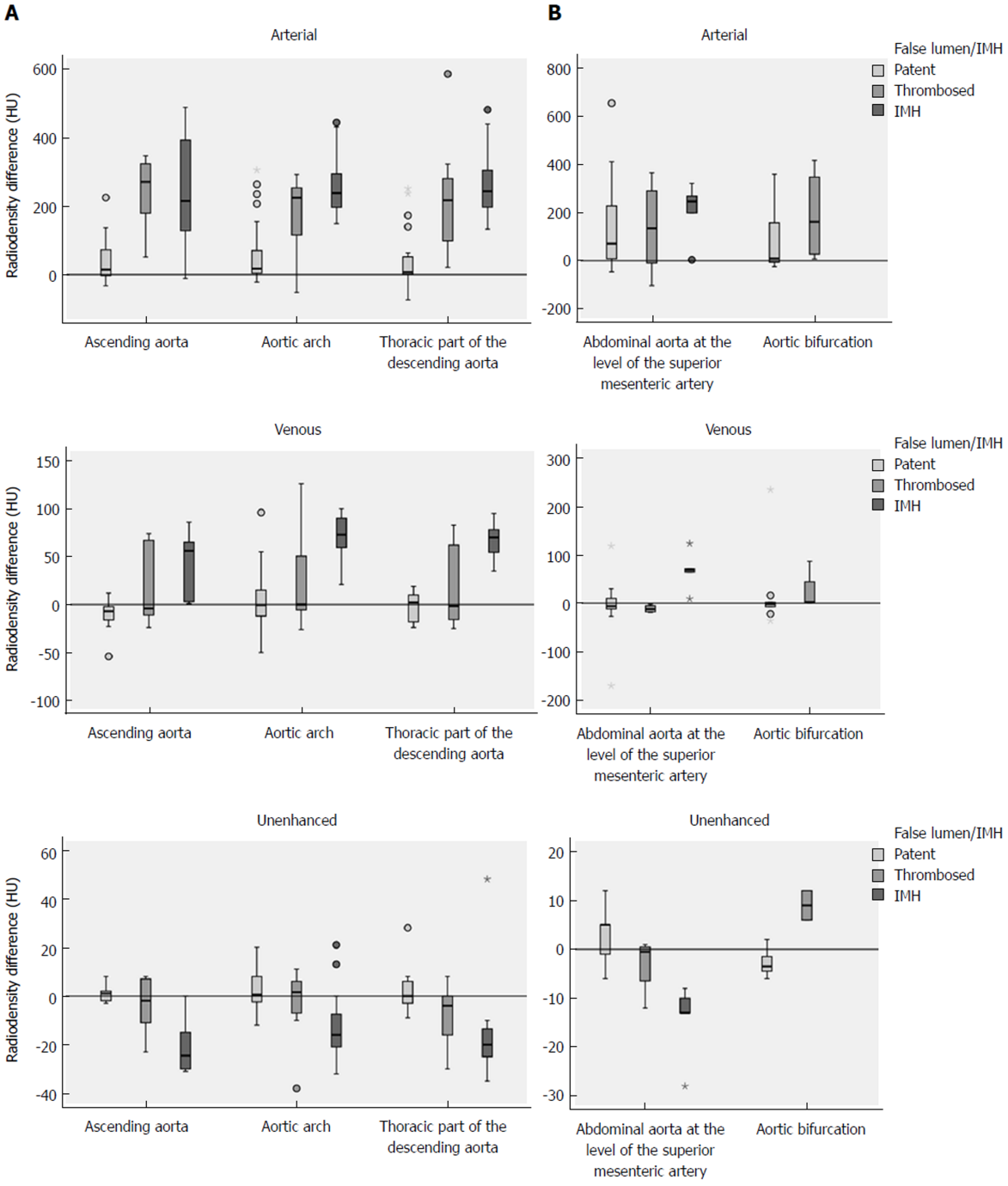

Figure 5 Density measurements, differences. Density differences between true and false lumen/intramural hematoma (IMH) in arterial, venous and unenhanced phase of (A) thoracic and (B) abdominal aorta. Differences in radiodensity between true lumen and IMH as well as true lumen and thrombosed false lumen, respectively, were only significant in the unenhanced acquisition ($P = 0.035$). IMH: Intramural hematoma.

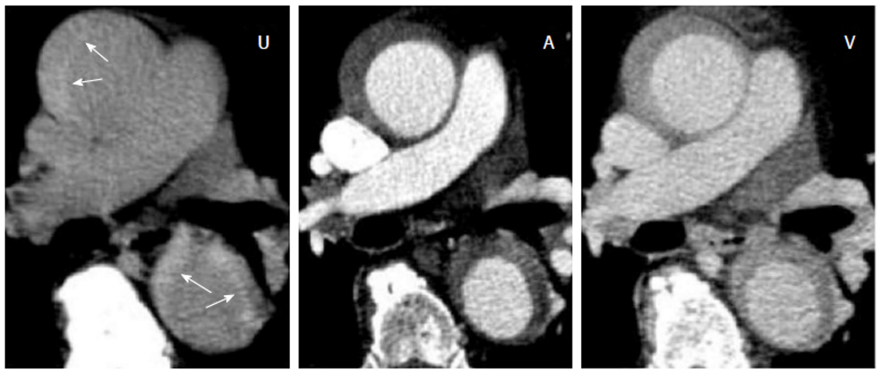

Figure 6 Acute intramural hematoma. Triphasic computed tomography angiography with an acute intramural hematoma (IMH) type Stanford A in the ascending and descending aorta. The unenhanced scan (U) shows a hyperdense wall thickening compared to the lumen (arrows). In the arterial (A) and venous (V) phase of the enhanced scans, the IMH con not be differentiated from a thrombotic layer.

ARTICLE HIGHLIGHTS

Research background

The life-threatening condition of an intramural hematoma (IMH) is often missed on routinely performed contrast enhanced computed tomography (CT) angiographies (CTA) in patients with suspected acute aortic syndrome (AAS).

Research motivation

To optimize the CT protocol for AAS.

Research objectives

To assess the potential benefit of a CTA protocol that includes an additional unenhanced acquisition added to contrast-enhanced scans in the diagnostic pathway of patients with AAS.

Research methods

Aortic CTA of patients with suspected AAS were retrospectively evaluated for acute aortic dissection, IMH, or penetrating aortic ulcer. The spiral CTA protocol consisted of an unenhanced acquisition and an arterial phase. If AAS was detected, a venous phase (delay, 90 s) was added. Images were evaluated for the presence and extent of aortic pathologies, and related complications.

Research results

23% of patients with AAS had an IMH. There was no significant difference in the involvement of the ascending aorta or the average age between dissection and IMH. Only the unenhanced acquisitions showed a significant density difference between the adjacent lumen and the IMH. Subadventitial hematoma involving the pulmonary trunk was present in five patients.

Research conclusions

IMH is a common and difficult to detect entity of AAS. An additional unenhanced acquisition within an aortic CTA protocol facilitates the detection of IMH.

Research perspectives

The results underline the importance of a triphasic CTA as standard diagnostic procedure in patients with suspected AAS.

REFERENCES

1 **Hallinan JT**, Anil G. Multi-detector computed tomography in the diagnosis and management of acute aortic syndromes. *World J Radiol* 2014; **6**: 355-365 [PMID: 24976936 DOI: 10.4329/wjr.v6.i6.355]
2 **Mészáros I**, Mórocz J, Szlávi J, Schmidt J, Tornóci L, Nagy L, Szép L. Epidemiology and clinicopathology of aortic dissection. *Chest* 2000; **117**: 1271-1278 [PMID: 10807810 DOI: 10.1378/chest.117.5.1271]
3 **Achenbach S**, Barkhausen J, Beer M, Beerbaum P, Dill T, Eichhorn J, Fratz S, Gutberlet M, Hoffmann M, Huber A. [Consensus recommendations of the German Radiology Society (DRG), the German Cardiac Society (DGK) and the German Society for Pediatric Cardiology (DGPK) on the use of cardiac imaging with computed tomography and magnetic resonance imaging]. *Rofo* 2012; **184**: 345-368 [PMID: 22426867 DOI: 10.1055/s-0031-1299400]
4 **Chao CP**, Walker TG, Kalva SP. Natural history and CT appearances of aortic intramural hematoma. *Radiographics* 2009; **29**: 791-804 [PMID: 19448116 DOI: 10.1148/rg.293085122]
5 **McMahon MA**, Squirrell CA. Multidetector CT of Aortic Dissection: A Pictorial Review.

Radiographics 2010; **30**: 445-460 [PMID: 20228328 DOI: 10.1148/rg.302095104]
6 **Daily PO**, Trueblood HW, Stinson EB, Wuerflein RD, Shumway NE. Management of acute aortic dissections. *Ann Thorac Surg* 1970; **10**: 237-247 [PMID: 5458238 DOI: 10.1016/S0003-4975(10)65594-4]
7 **Castañer E**, Andreu M, Gallardo X, Mata JM, Cabezuelo MA, Pallardó Y. CT in nontraumatic acute thoracic aortic disease: typical and atypical features and complications. *Radiographics* 2003; **23** Spec No: S93-110 [PMID: 14557505 DOI: 10.1148/rg.23si035507]
8 **Coady MA**, Rizzo JA, Elefteriades JA. Pathologic variants of thoracic aortic dissections. Penetrating atherosclerotic ulcers and intramural hematomas. *Cardiol Clin* 1999; **17**: 637-657 [PMID: 10589337 DOI: 10.1016/S0733-8651(05)70106-5]
9 **Tsai TT**, Nienaber CA, Eagle KA. Acute aortic syndromes. *Circulation* 2005; **112**: 3802-3813 [PMID: 16344407 DOI: 10.1161/CIRCULATIONAHA.105.534198]
10 **Song JK**, Yim JH, Ahn JM, Kim DH, Kang JW, Lee TY, Song JM, Choo SJ, Kang DH, Chung CH. Outcomes of patients with acute type a aortic intramural hematoma. *Circulation* 2009; **120**: 2046-2052 [PMID: 19901188 DOI: 10.1161/CIRCULATIONAHA.109.879783]
11 **Erbel R**, Aboyans V, Boileau C, Bossone E, Bartolomeo RD, Eggebrecht H, Evangelista A, Falk V, Frank H, Gaemperli O. 2014 ESC Guidelines on the diagnosis and treatment of aortic diseases: Document covering acute and chronic aortic diseases of the thoracic and abdominal aorta of the adult. The Task Force for the Diagnosis and Treatment of Aortic Diseases of the European Society of Cardiology (ESC). *Eur Heart J* 2014; **35**: 2873-2926 [PMID: 25173340 DOI: 10.1093/eurheartj/ehu281]
12 Statistikamt Nord. Bevölkerung der Gemeinden in Schleswig-Holstein. Available from: http://www.statistik-nord.de/daten/bevoelkerung-und gebiet/bevoelkerungsstand-und entwicklung/dokumentenansicht/163/produkte-1
13 **Harris KM**, Braverman AC, Eagle KA, Woznicki EM, Pyeritz RE, Myrmel T, Peterson MD, Voehringer M, Fattori R, Januzzi JL. Acute aortic intramural hematoma: an analysis from the International Registry of Acute Aortic Dissection. *Circulation* 2012; **126**: S91-S96 [PMID: 22965999 DOI: 10.1161/CIRCULATIONAHA.111.084541]

P- Reviewer: Abdelghany M, Benson RA, Okutucu S
S- Editor: Wang JL **L- Editor:** A **E- Editor:** Huang Y

World Journal of Radiology

Submit a Manuscript: https://www.f6publishing.com

World J Radiol 2018 November 28; 10(11): 162-171

DOI: 10.4329/wjr.v10.i11.162

ISSN 1949-8470 (online)

ORIGINAL ARTICLE

Retrospective Study

New scoring system in assessment of Hoffa's fat pad synovitis: A comparative study with established scoring systems

Shigeo Hagiwara, Albert Yang, Shoichiro Takao, Yasuhito Kaneko, Taiki Nozaki, Hiroshi Yoshioka

ORCID number: Shigeo Hagiwara (0000-0002-2734-8408); Albert Yang (0000-0002-2053-8460); Shoichiro Takao (0000-0002-8851-9813); Yasuhito Kaneko (0000-0001-8607-0197); Taiki Nozaki (0000-0002-1922-4085); Hiroshi Yoshioka (0000-0003-2686-1397).

Author contributions: Yoshioka H involved in overseeing the data collection process and data analysis following the data collection; Hagiwara S and Takao S accessed to subject identifiable data and analyzed the data; all the authors have read the manuscript and have approved this submission.

Institutional review board statement: The research protocol of this retrospective study was in compliance with the Helsinki Declaration, was approved by the institutional review board, and was registered with the University of California Irvine Medical Center.

Conflict-of-interest statement: No conflict of interest to be disclosed.

Shigeo Hagiwara, Albert Yang, Shoichiro Takao, Yasuhito Kaneko, Taiki Nozaki, Hiroshi Yoshioka, Department of Radiological Sciences, University of California Irvine Medical Center, Orange, CA 92868, United States

Abstract

AIM

To investigate the reliability of the established and new scoring methods for Hoffa's fat pad synovitis using magnetic resonance imaging (MRI).

METHODS

A total of 139 knees of 115 patients who underwent MRI of the knee with and without gadolinium contrast were enrolled in this study. Proton density (PD)-weighted, PD-weighted fat-suppressed (PD-FS), and postcontrast T1-weighted fat-suppressed (T1CE) images were used for evaluation. Using contrast and non-contrast images, our grading method for synovitis was performed to measure synovial thickness and signal intensity changes of the fat pad [Synovial membrane (SM) score], which was compared with the established methods, including MRI Osteoarthritis Knee Score (MOAKS), parapatellar synovitis score, Whole-Organ Magnetic Resonance Imaging Score (WORMS), and suprapatellar effusion diameter. Intraclass correlation coefficients (ICC) for intra and interobserver reproducibility and Spearman correlation coefficients (r) were calculated for the parapatellar synovitis score and each scoring method.

RESULTS

All of the scores presented substantial to almost perfect intrareliability. Among three readers, effusion diameter had substantial to almost perfect interreliability (ICC = 0.68-0.81) and WORMS had substantial interreliability (ICC = 0.61-0.70). For two out of three readers, there was substantial interreliability for the thickness score in T1CE (ICC = 0.55-0.69), SM scores in T1CE (ICC = 0.56-0.78) and PD-FS (ICC = 0.51-0.79), and parapatellar synovitis score in T1CE (ICC = 0.53-0.72). The parapatellar synovitis score was significantly correlated with the thickness score in T1CE (r = 0.70) and the SM score in T1CE (r = 0.81) and PD-FS (r = 0.65).

CONCLUSION

The newly proposed quantitative thickness score on T1CE and the semi-quantitative SM score on T1CE and PD-FS can be useful for Hoffa's fat pad synovitis.

Manuscript source: Unsolicited manuscript

Correspondence to: Hiroshi Yoshioka, MD, PhD, Chief Doctor, Professor, Executive Vice Chair, Department of Radiological Sciences, University of California Irvine Medical Center, 101 The City Drive South, Orange, CA 92868, United States.
hiroshi@uci.edu
Telephone: +1-877-8243627

Received: August 4, 2018
Peer-review started: August 5, 2018
First decision: August 24, 2018
Revised: September 22, 2018
Accepted: October 6, 2018
Article in press: October 6, 2018
Published online: November 28, 2018

Key words: Magnetic resonance imaging; Hoffa's fat pad synovitis; Semiquantitative score; Quantitative score; Scoring system

Core tip: We proposed a new grading method for Hoffa's fat pad synovitis and compared it with the other established methods. Our method showed substantial to almost perfect reproducibility and significant correlations with the established methods for both non-contrast and contrast images. Our newly proposed scoring system method can be useful for Hoffa's fat pad synovitis.

Hagiwara S, Yang A, Takao S, Kaneko Y, Nozaki T, Yoshioka H. New scoring system in assessment of Hoffa's fat pad synovitis: A comparative study with established scoring systems. *World J Radiol* 2018; 10(11): 162-171
URL: https://www.wjgnet.com/1949-8470/full/v10/i11/162.htm
DOI: https://dx.doi.org/10.4329/wjr.v10.i11.162

INTRODUCTION

Osteoarthritis (OA) of the knee is one of the most common chronic disorders that result in pain, deformity, and loss of function. OA has long been considered a wear and tear disease that leads to loss of cartilage because of mechanical stress. Recent experimental data have shown that OA is a complex disease with inflammatory mediators, which are released by cartilage, bone, and synovial fat pad[1-3].

The Hoffa's fat pad is located in the knee between the patellar tendon, femoral condyle, and tibial plateau. It is adjacent to the synovial layers and the cartilage surface of the femur[4]. Similar to subcutaneous tissue, the Hoffa's fat pad contains a framework of fibrous cords interspersed among adipose tissue[5] and is thought to distribute the synovial fluid and absorb forces through the knee joint[6]. Several studies have revealed that the fat pad produces growth factors and proinflammatory cytokines, which may contribute to the pathologic development of OA[7-9].

Several semiquantitative methods using magnetic resonance imaging (MRI) for the assessment of knee OA have been developed and used in various observational studies and clinical trials; by dividing the knee into subregions for assessment, these methods enable visualization of structures, such as the synovium, joint effusion, and cartilage[10,11]. Although each method have been reported to be clinically useful, the reliability was not perfect[12-14], and the scoring for Hoffa's fat pad synovitis based on non-enhanced sequences has not been sufficient, compared with that for the other subregions of the knee[10,11]. Although enhanced sequences allow for better characterization of synovial inflammation and for differentiation between the synovium and effusion, few scoring methods have been reported to be specific to Hoffa's fat pad synovitis[15,16]. Also, a routine knee MRI is usually obtained without contrast administration.

The aim of this study was to evaluate reliability of the established and new scoring methods, including non-enhanced MRI, for Hoffa's fat pad synovitis.

MATERIALS AND METHODS

Study design and subjects

The subjects enrolled in this study were all patients who underwent knee MRI with and without Gadolinium (Gd) contrast at our institute from January 2012 to July 2015. During this period, MRI of the knee with and without Gd contrast was performed on 205 knees (102 on the right, 103 on the left) of 168 patients. The exclusion criteria of this study were as follows: (1) under 18 years old; (2) postoperation with an implant around the knee; (3) inflammatory arthritis, such as rheumatoid arthritis and infection; (4) acute trauma with hemarthrosis; (5) intraarticular tumor; (6) difficult evaluation due to severe deformity from OA or amputation; and (7) difficult evaluation due to severe artifact. After exclusion of 66 knees of 53 patients, a total of 139 knees (69 on the right, 70 on the left) of 115 patients available for analyses. The subjects had an average age of 54 years.

The research protocol of this retrospective study was in compliance with the Helsinki Declaration, was approved by the institutional review board, and was registered with the University of California Irvine Medical Center.

MRI protocol

Each MRI examination in this study was performed according to a standardized institutional protocol using the 1.5T (Avanto, Siemens Healthcare, Erlangen, Germany) or the 3T MRI system (Achieva or dStream Achieva, Philips Healthcare, Best, Netherland and TtioTim, Siemens Healthcare); 42 knees underwent MRI with 1.5T and 97 knees with 3T. A non-enhanced proton density (PD)-weighted fast spin-echo sequence was performed in the sagittal plane, followed by non-enhanced PD-weighted fat-suppressed (PD-FS) fast spin-echo sequence in the sagittal and axial planes. After injection of 10 mL of Gd contrast (Multihance, Bracco) into a peripheral vein, T1-weighted fat-suppressed fast spin-echo sequence (T1CE) was performed in the sagittal and axial planes. The imaging parameters of all sequences are summarized in Table 1.

MRI assessment

The MRI evaluation of synovitis and joint effusion was performed independently by a board-certified orthopedic surgeon (A), who had 10 years of experience, and two radiology residents (B, C), who had 2 years of experience each. All readers were blinded to the clinical information but not to the MR sequences, because the imaging characteristics were readily apparent to the observer. To evaluate intraobserver reliability, a second trial was performed by Hagiwara S four weeks later.

Synovial evaluation

Thickness score: For the new quantitative scoring system, the thickness of the inflamed synovium was determined as the area of enhancement along the posterior Hoffa's fat pad on sagittal T1CE, as low-signal regions on non-enhanced sagittal PD, and as high-signal regions on non-enhanced sagittal PD-FS. Three sagittal slices, including the medial and lateral aspects of the Hoffa's fat pad and the central patellofemoral groove, were chosen. In each slice, three points (*i.e.*, proximal, middle, and distal) along the posterior surface of Hoffa's fat pad were selected. The average thickness of the synovium from the nine points in each sequence (Figure 1) was graded on a three-point scale: grade 1 ≤ 0.8 mm; grade 2 = 0.8 mm to 1.6 mm; and grade 3 ≥ 1.6 mm.

Synovial membrane score (SM score): The contrast effects and signal intensity changes along the posterior surface of the Hoffa's fat pad on a single sagittal slice through the central patellofemoral groove were used to semiquantitatively grade the synovitis. The score was based on the contrast effects and signal intensity changes[17] on sagittal T1CE; low-signal areas on sagittal PD; and high-signal areas on sagittal PD-FS. The score was graded on a four-point scale as grade 0 for lack of enhancement or signal change; grade 1 for the presence of a linear contrast effect or signal change on the posterior fat pad synovium; grade 2 for the presence of a nodular contrast effect or signal change on the posterior fat pad and/or mild exudation of the fat pad on T1CE; and grade 3 for gross a nodular contrast effect or signal change on the posterior fat pad and/or severe exudation of the fat pad on T1CE, as seen on the sagittal plane at the center of the patella (Figure 2).

MRI Osteoarthritis Knee Score (MOAKS) for fat pad: Hoffa's synovitis was scored with the MOAKS system[11] by grading the size of the diffuse hyperintense signal in the Hoffa's fat pad on T1CE and PD-FS on a four-point scale, as follows: 0 = normal; 1 = mild, 2 = moderate, 3 = severe.

Parapatellar synovitis score: Synovial inflammation in the entire knee was scored, as previously reported[18]. These parapatellar sites included three in the suprapatellar recesses (*i.e.*, lateral, medial, and just above the trochlear groove), as well as the medial and lateral femoral gutters. Thickening of the inflamed synovium was determined in each site and was scored on a four-point scale, according to the thickness, as grade 0 for lack of enhancement of the synovial tissue; grade 1 for < 2-mm thickening of the synovial tissue; grade 2 for 2-4-mm thickening of the synovial tissue; and grade 3 for > 4-mm thickening or nodular pattern of the synovial tissue (Figure 3).

Effusion evaluation

Effusion diameter: Joint effusion was assessed based on the greatest diameter of the fluid accumulation, perpendicular to the long axis of the leg on non-enhanced PD-FS, as follows; grade 0, < 5 mm; grade 1, between 5 mm and 10 mm; grade 2, between 10

Table 1 Magnetic resonance imaging parameters for the sequences

Imaging parameter	Tesla	Sequence				
		Sag PD	Sag PD-FS	Sag T1CE	Ax PD-FS	Ax T1CE
Repetition time (ms)	1.5T	2000	3000	438	3400	714
	3T	2054-3940	3000-4150	530-782	3000-5300	530-782
Echo time (ms)	1.5T	46	46	12	43	13
	3T	22-30	30-43	12-20	13-45	12-20
Matrix resolution (mm)	1.5T	0.7 × 0.7	0.7 × 0.7	0.7 × 0.7	0.6 × 0.6	0.6 × 0.6
	3T	0.3 × 3.3	0.3 × 0.3	0.3 × 0.3	0.3 × 0.3	0.3 × 0.3
Field of view (mm)	1.5T	150	150	150	150	150
	3T	150	150	150	150	150
Slice thickness (mm)	1.5T	3.5	3.5	3.5	5	5
	3T	2.5	2.5	2.5	3	3

Sag PD: Sagittal proton density-weighted sequence; Sag PD-FS: Sagittal proton density-weighted fat-suppressed sequence; Sag T1CE: Sagittal contrast-enhanced T1-weighted fat-suppressed sequence; Ax PD-FS: Axial proton density-weighted fat-suppressed sequence; Ax T1CE: Axial contrast-enhanced T1-weighted fat-suppressed sequence; T1CE: T1-weighted fat-suppressed fast spin-echo sequence; PD: Proton density-weighted fast spin-echo sequence; PD-FS: Proton density-weighted fat-suppressed fast spin-echo sequence.

mm and 20 mm; and grade 3, > 20 mm[19].

Whole-Organ Magnetic Resonance Imaging Score (WORMS) for synovial effusion: Synovial effusion was evaluated to describe the synovitis according to the WORMS system[10]. Joint effusion was graded collectively from 0 to 3 in terms of the percentage of the estimated maximal distention of the synovial cavity, as follows: grade 0, normal; grade 1, < 33%; grade 2, 33% to 66%; and grade 3, > 66%.

Statistical analysis

Statistical analysis was performed by the biostatistics service of our institute using MedCalc software (Ver.16, MedCalc Software, Ostend, Belgium). The inter and intraobserver reliabilities of each score were assessed using intraclass correlation coefficient (ICC) analysis. An ICC of 0.2-0.4 was considered as fair, 0.4-0.6 as moderate, 0.6-0.8 as substantial, and 0.8-1 as almost perfect[20]. Spearman's rank correlation (*r*) was computed to analyze the correlation between each scoring system and the MOAKS score, which was the most popular MRI semiquantitative scoring system for OA[14]. Because an adequate correlation between the parapatellar synovitis score and arthroscopic and microscopic scoring has been reported[21,22], the correlations of the parapatellar synovitis score with each scoring system were computed on 1.5T and 3T, respectively. Correlation was considered negligible for a *r* value < 0.2, low for a *r* value of 0.2-0.4, moderate for a *r* value of 0.4-0.7, strong for a *r* value of 0.7-0.9, and very strong for a *r* value > 0.9[23].

RESULTS

Reproducibility of the scoring systems

The ICCs for inter and intraobserver reliabilities of each score are shown in Table 2. All of the scores had substantial to almost perfect intrareliability. Among the three readers, interreliability was substantial to almost perfect for effusion diameter (ICC = 0.68-0.81) and substantial for WORMS (ICC = 0.61-0.70). For two out of three readers, there was substantial interreliability for the thickness score in T1CE (ICC = 0.55-0.69), SM scores in T1CE (ICC = 0.56-0.78) and PD-FS (ICC = 0.51-0.79), and parapatellar synovitis score in T1CE (ICC = 0.53-0.72).

Correlation with the standard

The Spearman's rank correlation results for the MOAKS are shown in Table 3. On the average, the MOAKS had moderate to strong correlations with each scoring system (*r* = 0.44-0.71). The correlations of each scoring system with the parapatellar synovitis score are shown in Table 4. The parapatellar synovitis score had nearly strong correlations with the thickness score in T1CE (*r* = 0.70), SM score in T1CE (*r* = 0.81), and SM score in PD-FS (*r* = 0.65). There were no significant differences between the

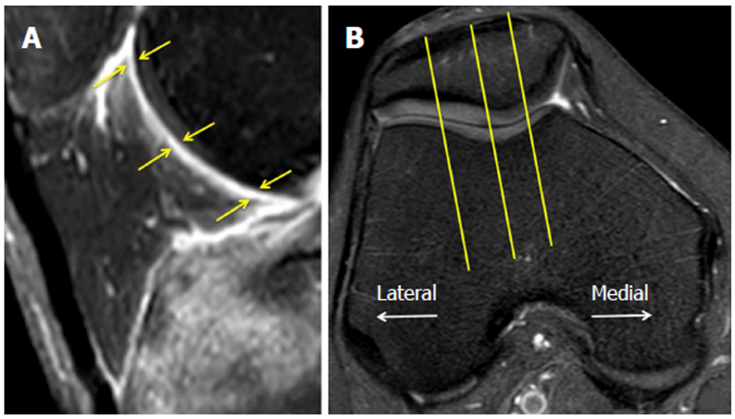

Figure 1 Thickness score. A: The thickness of Hoffa's synovitis is measured at three points at the proximal, middle, and distal synovium along the posterior aspect of the Hoffa's fat pad (yellow arrow); B: Sagittal slices are selected at the medial, lateral, and central patellofemoral groove.

1.5T and 3T sequences.

Figure 4 demonstrates a case with similar scores for Hoffa's synovitis among the PD-FS, PD, and T1CE, whereas Figure 5 demonstrates a case with different PD-FS, PD, and T1CE scores.

DISCUSSION

This study compared the established scoring methods, including the MOAKS score for fat pad, parapatellar synovitis score, WORMS scoring for synovial effusion, and effusion diameter, and the new scoring methods, including the thickness score and SM score for Hoffa's fat pad synovitis. The thickness score and the SM score demonstrated almost equal reproducibility with that of the other scoring systems and were superior to the MOAKS. The associations of the thickness score and the SM score with the MOAKS score were equal with that of the other scoring systems. Furthermore, the parapatellar synovitis score had strong associations with the thickness score in T1CE and the SM scores in T1CE and PD-FS.

Although the MOAKS score is based on the size and degree of hyperintensity on T2/ intermediate-weighted imaging or on the PD-FS within the Hoffa's fat pad[11], it does not clearly define the size and the slice delineation. This may have contributed to the relatively low interreliability for the MOAKS sore in this study. On the other hand, in the WORMS study, interobserver reliability was substantial despite the subjective analysis of the synovial cavity[10]. By evaluating both synovial tissue and fluid, even without clearly distinguishing between the two entities[10], the WORMS system can reliably evaluate the severity of the synovitis. In this study, there was substantial to almost perfect inter and intrareliability for the effusion diameter scoring, likely because measurement of the anterior to posterior dimensions of the joint fluid was straightforward and experience on orthopedic surgery or radiology was not always necessary.

The reliability of the thickness score in T1CE was better than in PD and PD-FS. An advantage of contrast-enhanced MRI is the ability to distinguish synovial inflammation from synovial fluid and fat tissues[20,24]. Guermazi *et al*[25] reported excellent reproducibility using a contrast-enhanced whole-knee synovitis scoring system. In non-contrast sequences, the border of the intensity change of synovitis is difficult to accurately recognize; this can be one of the reasons for the relatively low inter and intrareliability for the non-contrast analyses of the thickness score. The additional problems of the thickness score in T1CE were fragmentation and contrast exudation of the fat pad, which might have significantly increased the variability in measurement and, in severe cases, overestimated synovitis. The SM score is based on a well-known scoring method for synovitis of the wrist[17,26]. In this method, the high-intensity change seems easy to recognize in both T1CE and PD-FS.

Because the MOAKS enables visualization of the signal intensity change within the Hoffa's fat pad in asymptomatic patients[27], it was thought to be a sensitive but non-specific finding for synovitis[24]. This was a possible reason for the relatively low correlations between the MOAKS and the other scoring methods. Although the parapatellar synovitis score evaluates a region of interest that is different from the

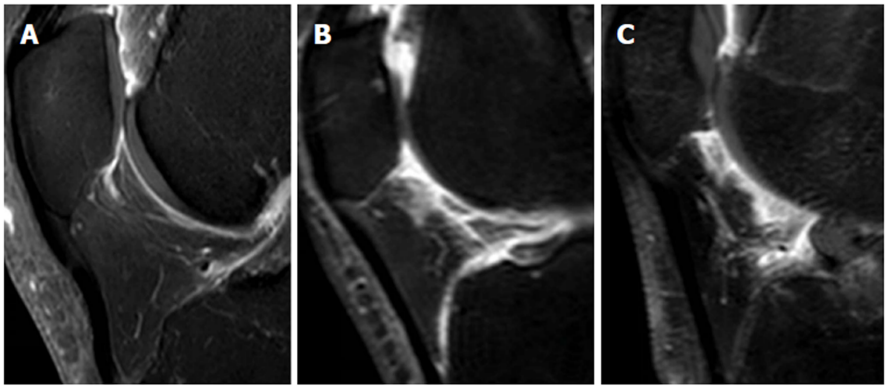

Figure 2 Grading of the Synovial membrane score. A: Grade1 is defined as linear thickening of the posterior Hoffa's fat pad's synovium; B: Grade 2 is defined as mild exudation and signal change in the posterior Hoffa's fat pad; C: Grade 3 is defined as gross nodular thickening of the posterior Hoffa's fat pad's synovium.

Hoffa's fat pad, it can be the standard of this study, considering its correlation with the arthroscopic and microscopic scoring of the knee and its previously reported correlation with the WORMS score of the fat pad[21,22]. The thickness score in T1CE and the SM scores in T1CE and PD-FS had strong associations with the parapatellar synovitis score. This suggested that evaluation of synovitis using the SM score on PD-FS had a similar reliability with that of a contrast-enhanced study. Although most contrast studies for synovitis were based on synovial thickness[15,22], this semiquantitative method can simply evaluate both the intensity change on the posterior fat pad and exudation to the fat pad. Due to concerns of increased cost and risk from contrast injection[11], the SM score in PD-FS may provide a viable alternative to contrast-enhanced examinations for the evaluation of Hoffa's fat pad synovitis.

Several limitations of this study should be acknowledged. First, we did not compare the scores with arthroscopic and microscopic examinations as the standard, because the current study was retrospective and most subjects were not in preoperative status. Second, the parapatellar synovitis score was not a specific scoring method for Hoffa's fat pad. Despite this, ample correlation of the parapatellar synovitis score with the arthroscopic and microscopic scoring had been demonstrated[19,20]. Third, there was variability in experience among the readers who interpreted the knee MRIs. Although two junior radiology residents were included, there was no significant difference in the scoring results among the readers. This suggested that our methods would be available for many physicians who may not be familiar with knee MRI interpretation. Finally, the use of both 1.5T and 3T MRI systems in this study may have produced variability in the tissue contrast on the PD or PD-FS images and in the degree of contrast enhancement on T1CE images, thereby, affecting the scoring for Hoffa's synovitis.

In conclusion, the newly proposed quantitative thickness score on T1CE and the semiquantitative SM scores on T1CE and PD-FS can be useful for Hoffa's fat pad synovitis. Semiquantiative scoring on PD-FS sequences may be a reliable surrogate to contrast-enhanced assessment of Hoffa's fat pad synovitis.

Table 2 Inter and intraobserver reliability

		Intra-observer	Inter-observer		
		A1-A2	A1-B	A1-C	B-C
Thickness	T1CE	0.74 (0.65-0.81)	0.69 (0.60-0.77)	0.67 (0.56-0.75)	0.55 (0.42-0.65)
	PD	0.68 (0.58-0.76)	0.45 (0.31-0.57)	0.49 (0.35-0.61)	0.54 (0.41-0.65)
	PD-FS	0.71 (0.61-0.78)	0.59 (0.48-0.69)	0.49 (0.35-0.60)	0.63 (0.52-0.72)
SM score	T1CE	0.88 (0.83-0.91)	0.67 (0.56-0.75)	0.78 (0.70-0.83)	0.56 (0.43-0.66)
	PD	0.88 (0.83-0.91)	0.49 (0.35-0.60)	0.72 (0.63-0.79)	0.50 (0.36-0.61)
	PD-FS	0.89 (0.85-0.92)	0.51 (0.38-0.63)	0.79 (0.71-0.84)	0.62 (0.50-0.71)
MOAKS	T1CE	0.76 (0.68-0.82)	0.64 (0.53-0.73)	0.54 (0.41-0.65)	0.49 (0.35-0.60)
Synovitis-score	T1CE	0.93 (0.91-0.95)	0.65 (0.54-0.74)	0.72 (0.62-0.79)	0.53 (0.40-0.64)
WORMS (effusion synovitis)	PD-FS	0.77 (0.70-0.83)	0.70 (0.61-0.78)	0.61 (0.50-0.71)	0.68 (0.58-0.76)
Effusion-diameter	PD-FS	0.89 (0.85-0.92)	0.77 (0.69-0.83)	0.81 (0.75-0.86)	0.68 (0.58-0.76)

Data are presented as ICC (95%CI). T1CE: T1-weighted fat-suppressed fast spin-echo sequence; PD: Proton density-weighted fast spin-echo sequence; PD-FS: Proton density-weighted fat-suppressed fast spin-echo sequence.

Table 3 Correlation with the MOAKS score

		1.5T	3T	Total
Thickness	T1CE	0.45	0.49	0.47
	PD	0.32	0.49	0.44
	PD-FS	0.42	0.41	0.41
SM score	T1CE	0.55	0.68	0.64
	PD	0.61	0.64	0.63
	PD-FS	0.64	0.74	0.71
Synovitis-score	T1CE	0.68	0.51	0.56
WORMS (effusion synovitis)	PD-FS	0.48	0.55	0.53
Effusion-diameter	PD-FS	0.58	0.48	0.51

All *P* values are less than 0.01. T1CE: T1-weighted fat-suppressed fast spin-echo sequence; PD: Proton density-weighted fast spin-echo sequence; PD-FS: Proton density-weighted fat-suppressed fast spin-echo sequence.

Table 4 Correlation with the parapatellar synovitis score

		1.5T	3T	Total
Thickness	T1CE	0.63	0.73	0.70
	PD	0.52	0.45	0.47
	PD-FS	0.44	0.51	0.49
SM score	T1CE	0.85	0.79	0.81
	PD	0.42	0.76	0.66
	PD-FS	0.79	0.59	0.65
MOAKS	T1CE	0.66	0.56	0.59
	PD-FS	0.65	0.52	0.56
WORMS (effusion synovitis)	PD-FS	0.64	0.81	0.76
Effusion-diameter	PD-FS	0.52	0.62	0.59

All *P* values are less than 0.01. T1CE: T1-weighted fat-suppressed fast spin-echo sequence; PD: Proton density-weighted fast spin-echo sequence; PD-FS: Proton density-weighted fat-suppressed fast spin-echo sequence.

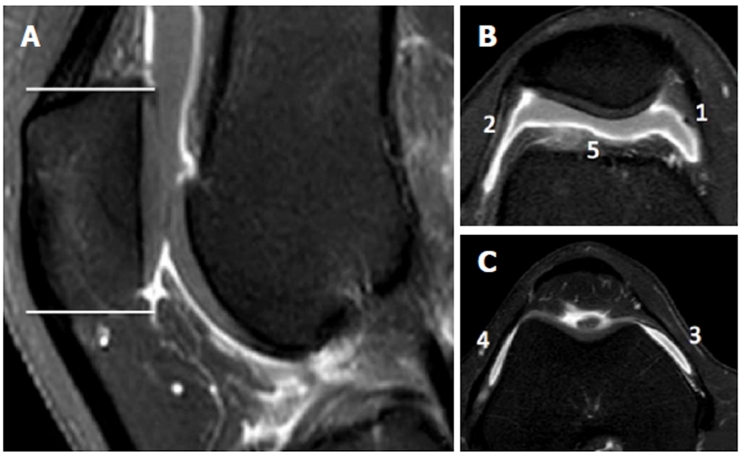

Figure 3 Parapatellar synovitis score. A: Two slices are chosen for the parapatellar synovitis score, and each corresponds with the first and last axial slice, respectively, in which the patella was still visible; B, C: The five sites of interest include three points in the suprapatellar recess, one point in the lateral gutter, and one point in the medial femoral gutter. Thickening of the inflamed synovium is determined in each site and is graded on a four-point scale, according to the thickness.

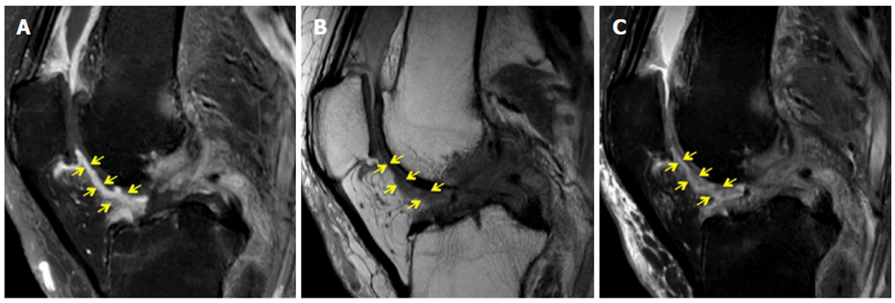

Figure 4 A 69-year-old woman with osteoarthritis and a parapatellar score of 9. A: The thickness score is grade 3, the Synovial membrane (SM) score is grade 3, and the MOAKS score is grade 3 on T1-weighted fat-suppressed fast spin-echo sequence; B: The thickness score is grade 2, the SM score is grade 3, and the MOAKS score is grade 3 on proton density-weighted fast spin-echo sequence; C: The thickness score is grade 3, the SM score is grade 3, and the MOAKS score is grade 3 on proton density-weighted fat-suppressed fast spin-echo sequence.

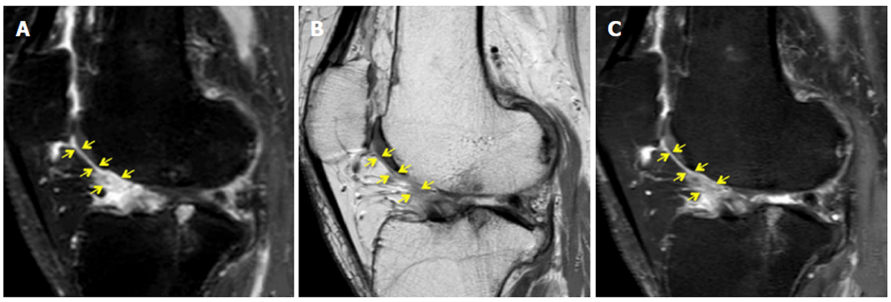

Figure 5 A 71-year-old woman with osteoarthritis and a parapatellar score of 8. A: The thickness score is grade 2, the Synovial membrane (SM) score is grade 3, and the MOAKS score is grade 3 on T1-weighted fat-suppressed fast spin-echo sequence; B: The thickness score is grade 1, the SM score is grade 1, and the MOAKS score is grade 3 on proton density-weighted fast spin-echo sequence; C: The thickness score is grade 2, the SM score is grade 3, and the MOAKS score is grade 3 on proton density-weighted fat-suppressed fast spin-echo sequence.

ARTICLE HIGHLIGHTS

Research background

Osteoarthritis (OA) of the knee is one of the most common chronic disorders resulting in pain, deformity, and loss of function. Several semiquantitative methods using magnetic resonance imaging (MRI) for assessment of knee OA have been developed and used in various observational studies and clinical trials.

Research motivation
Although all assessment methods had been reported to be clinical useful, their reliability was not perfect, and the scoring for Hoffa's fat pad synovitis based on non-enhanced sequence has not been sufficient, compared with that for the other subregions of the knee.

Research objectives
The aim of this study was to evaluate the reliability of the established and new scoring methods, including non-enhanced MRI, for Hoffa's fat pad synovitis.

Research methods
This study enrolled 139 knees of 115 patients who underwent MRI of the knee with and without Gadolinium contrast. Proton density (PD)-weighted, proton density-weighted fat-suppressed (PD-FS), and postcontrast T1-weighted fat-suppressed (T1CE) images were used for evaluation. Our grading method for synovitis was performed using non-contrast and contrast images to measure synovial thickness and signal intensity changes of the fat pad (SM score). Intraclass correlation coefficients (ICC) for intra and interobserver reproducibility and the Spearman correlation coefficients (r) with the parapatellar synovitis score were calculated for each scoring method.

Research results
The thickness score in T1CE and the SM scores in T1CE and PD-FS showed substantial to almost perfect reproducibility. The parapatellar synovitis score statistically significant correlation with the thickness score in T1CE (r = 0.68) and thee SM scores in T1CE (r = 0.71) and PD-FS (r = 0.66).

Research conclusions
The newly proposed quantitative thickness score on T1CE and the semiquantitative SM scores on T1CE and PD-FS can be useful for Hoffa's fat pad synovitis.

Research perspectives
Our findings indicated that the established scoring systems for Hoffa's fat pad synovitis could be further improved. Future research may propose more reliable methods for Hoffa's fat pad synovitis.

ACKNOWLEDGMENTS

We would like to thank Maryam Soltanolkotabi, for helping us make the grading system, and all the staff of the Department of Radiological Sciences at the University of California Irvine, for helping in collecting the data and obtaining the MRI.

REFERENCES

1 **Kapoor M**, Martel-Pelletier J, Lajeunesse D, Pelletier JP, Fahmi H. Role of proinflammatory cytokines in the pathophysiology of osteoarthritis. *Nat Rev Rheumatol* 2011; **7**: 33-42 [PMID: 21119608 DOI: 10.1038/nrrheum.2010.196]
2 **Loeser RF**, Goldring SR, Scanzello CR, Goldring MB. Osteoarthritis: a disease of the joint as an organ. *Arthritis Rheum* 2012; **64**: 1697-1707 [PMID: 22392533 DOI: 10.1002/art.34453]
3 **Goldring MB**, Otero M. Inflammation in osteoarthritis. *Curr Opin Rheumatol* 2011; **23**: 471-478 [PMID: 21788902 DOI: 10.1097/BOR.0b013e328349c2b1]
4 **Hoffa A**. Influence of adipose tissue with regard to the pathology of the knee joint. *JAMA* 1904; **43**: 795-796
5 **Vahlensieck M**, Linneborn G, Schild H, Schmidt HM. Hoffa's recess: incidence, morphology and differential diagnosis of the globular-shaped cleft in the infrapatellar fat pad of the knee on MRI and cadaver dissections. *Eur Radiol* 2002; **12**: 90-93 [PMID: 11868081 DOI: 10.1007/s003300100982]
6 **Saddik D**, McNally EG, Richardson M. MRI of Hoffa's fat pad. *Skeletal Radiol* 2004; **33**: 433-444 [PMID: 15221217 DOI: 10.1007/s00256-003-0724-z]
7 **Ushiyama T**, Chano T, Inoue K, Matsusue Y. Cytokine production in the infrapatellar fat pad: another source of cytokines in knee synovial fluids. *Ann Rheum Dis* 2003; **62**: 108-112 [PMID: 12525378 DOI: 10.1136/ard.62.2.108]
8 **Distel E**, Cadoudal T, Durant S, Poignard A, Chevalier X, Benelli C. The infrapatellar fat pad in knee osteoarthritis: an important source of interleukin-6 and its soluble receptor. *Arthritis Rheum* 2009; **60**: 3374-3377 [PMID: 19877065 DOI: 10.1002/art.24881]
9 **Klein-Wieringa IR**, Kloppenburg M, Bastiaansen-Jenniskens YM, Yusuf E, Kwekkeboom JC, El-Bannoudi H, Nelissen RG, Zuurmond A, Stojanovic-Susulic V, Van Osch GJ. The infrapatellar fat pad of patients with osteoarthritis has an inflammatory phenotype. *Ann Rheum Dis* 2011; **70**: 851-857 [PMID: 21242232 DOI: 10.1136/ard.2010.140046]
10 **Peterfy CG**, Guermazi A, Zaim S, Tirman PF, Miaux Y, White D, Kothari M, Lu Y, Fye K, Zhao S. Whole-Organ Magnetic Resonance Imaging Score (WORMS) of the knee in osteoarthritis. *Osteoarthritis Cartilage* 2004; **12**: 177-190 [PMID: 14972335 DOI: 10.1016/j.joca.2003.11.003]
11 **Hunter DJ**, Guermazi A, Lo GH, Grainger AJ, Conaghan PG, Boudreau RM, Roemer FW. Evolution of semi-quantitative whole joint assessment of knee OA: MOAKS (MRI Osteoarthritis Knee Score). *Osteoarthritis Cartilage* 2011; **19**: 990-1002 [PMID: 21645627 DOI: 10.1016/j.joca.2011.05.004]
12 **Lynch JA**, Roemer FW, Nevitt MC, Felson DT, Niu J, Eaton CB, Guermazi A. Comparison of

BLOKS and WORMS scoring systems part I. Cross sectional comparison of methods to assess cartilage morphology, meniscal damage and bone marrow lesions on knee MRI: data from the osteoarthritis initiative. *Osteoarthritis Cartilage* 2010; **18**: 1393-1401 [PMID: 20816979 DOI: 10.1016/j.joca.2010.08.017]

13 **Felson DT**, Lynch J, Guermazi A, Roemer FW, Niu J, McAlindon T, Nevitt MC. Comparison of BLOKS and WORMS scoring systems part II. Longitudinal assessment of knee MRIs for osteoarthritis and suggested approach based on their performance: data from the Osteoarthritis Initiative. *Osteoarthritis Cartilage* 2010; **18**: 1402-1407 [PMID: 20851202 DOI: 10.1016/j.joca.2010.06.016]

14 **Roemer FW**, Hunter DJ, Crema MD, Kwoh CK, Ochoa-Albiztegui E, Guermazi A. An illustrative overview of semi-quantitative MRI scoring of knee osteoarthritis: lessons learned from longitudinal observational studies. *Osteoarthritis Cartilage* 2016; **24**: 274-289 [PMID: 26318656 DOI: 10.1016/j.joca.2015.08.011]

15 **Roemer FW**, Guermazi A, Zhang Y, Yang M, Hunter DJ, Crema MD, Bohndorf K. Hoffa's Fat Pad: Evaluation on Unenhanced MR Images as a Measure of Patellofemoral Synovitis in Osteoarthritis. *AJR Am J Roentgenol* 2009; **192**: 1696-1700 [PMID: 19457837 DOI: 10.2214/AJR.08.2038]

16 **Ballegaard C**, Riis RG, Bliddal H, Christensen R, Henriksen M, Bartels EM, Lohmander LS, Hunter DJ, Bouert R, Boesen M. Knee pain and inflammation in the infrapatellar fat pad estimated by conventional and dynamic contrast-enhanced magnetic resonance imaging in obese patients with osteoarthritis: a cross-sectional study. *Osteoarthritis Cartilage* 2014; **22**: 933-940 [PMID: 24821663 DOI: 10.1016/j.joca.2014.04.018]

17 **Ostergaard M**, Hansen M, Stoltenberg M, Gideon P, Klarlund M, Jensen KE, Lorenzen I. Magnetic resonance imaging-determined synovial membrane volume as a marker of disease activity and a predictor of progressive joint destruction in the wrists of patients with rheumatoid arthritis. *Arthritis Rheum* 1999; **42**: 918-929 [PMID: 10323447 DOI: 10.1002/1529-0131(199905)42:53.0.CO;2-2]

18 **Loeuille D**, Chary-Valckenaere I, Champigneulle J, Rat AC, Toussaint F, Pinzano-Watrin A, Goebel JC, Mainard D, Blum A, Pourel J. Macroscopic and microscopic features of synovial membrane inflammation in the osteoarthritic knee: correlating magnetic resonance imaging findings with disease severity. *Arthritis Rheum* 2005; **52**: 3492-3501 [PMID: 16255041 DOI: 10.1002/art.21373]

19 **Meredith DS**, Losina E, Neumann G, Yoshioka H, Lang PK, Katz JN. Empirical evaluation of the inter-relationship of articular elements involved in the pathoanatomy of knee osteoarthritis using magnetic resonance imaging. *BMC Musculoskelet Disord* 2009; **10**: 133 [PMID: 19874594 DOI: 10.1186/1471-2474-10-133]

20 **Landis JR**, Koch GG. The measurement of observer agreement for categorical data. *Biometrics* 1977; **33**: 159-174 [PMID: 843571]

21 **Loeuille D**, Rat AC, Goebel JC, Champigneulle J, Blum A, Netter P, Gillet P, Chary-Valckenaere I. Magnetic resonance imaging in osteoarthritis: which method best reflects synovial membrane inflammation? Correlations with clinical, macroscopic and microscopic features. *Osteoarthritis Cartilage* 2009; **17**: 1186-1192 [PMID: 19332177 DOI: 10.1016/j.joca.2009.03.006]

22 **Loeuille D**, Sauliere N, Champigneulle J, Rat AC, Blum A, Chary-Valckenaere I. Comparing non-enhanced and enhanced sequences in the assessment of effusion and synovitis in knee OA: associations with clinical, macroscopic and microscopic features. *Osteoarthritis Cartilage* 2011; **19**: 1433-1439 [PMID: 21930225 DOI: 10.1016/j.joca.2011.08.010]

23 **Guilford JP**. *Fundamental statistics in psychology and education*New York: McGraw Hill; 1956

24 **Crema MD**, Felson DT, Roemer FW, Niu J, Marra MD, Zhang Y, Lynch JA, El-Khoury GY, Lewis CE, Guermazi A. Peripatellar synovitis: comparison between non-contrast-enhanced and contrast-enhanced MRI and association with pain. The MOST study. *Osteoarthritis Cartilage* 2013; **21**: 413-418 [PMID: 23277189 DOI: 10.1016/j.joca.2012.12.006]

25 **Guermazi A**, Roemer FW, Hayashi D, Crema MD, Niu J, Zhang Y, Marra MD, Katur A, Lynch JA, El-Khoury GY. Assessment of synovitis with contrast-enhanced MRI using a whole-joint semiquantitative scoring system in people with, or at high risk of, knee osteoarthritis: the MOST study. *Ann Rheum Dis* 2011; **70**: 805-811 [PMID: 21187293 DOI: 10.1136/ard.2010.139618]

26 **Stomp W**, Krabben A, van der Heijde D, Huizinga TW, Bloem JL, Østergaard M, van der Helm-van Mil AH, Reijnierse M. Aiming for a simpler early arthritis MRI protocol: can Gd contrast administration be eliminated? *Eur Radiol* 2015; **25**: 1520-1527 [PMID: 25636414 DOI: 10.1007/s00330-014-3522-1]

27 **De Smet AA**, Davis KW, Dahab KS, Blankenbaker DG, del Rio AM, Bernhardt DT. Is there an association between superolateral Hoffa fat pad edema on MRI and clinical evidence of fat pad impingement? *AJR Am J Roentgenol* 2012; **199**: 1099-1104 [PMID: 23096185 DOI: 10.2214/AJR.12.8798]

P- Reviewer: Gheita TA, Jennane R
S- Editor: Wang JL **L- Editor:** A **E- Editor:** Huang Y

World Journal of Radiology

Submit a Manuscript: https://www.f6publishing.com

World J Radiol 2018 November 28; 10(11): 172-183

DOI: 10.4329/wjr.v10.i11.172

ISSN 1949-8470 (online)

ORIGINAL ARTICLE

Retrospective Study

High-resolution computed tomography findings in humoral primary immunodeficiencies and correlation with pulmonary function tests

Lorenzo Cereser, Marco De Carli, Paola d'Angelo, Elisa Zanelli, Chiara Zuiani, Rossano Girometti

ORCID number: Lorenzo Cereser (0000-0003-4480-8872); Marco De Carli (0000-0003-4845-205X); Paola d'Angelo (0000-0003-2218-5571); Elisa Zanelli (0000-0002-7271-0613); Chiara Zuiani (0000-0001-5132-3115); Rossano Girometti (0000-0002-0904-5147).

Author contributions: All authors helped performing the research; Cereser L drafted the concept of the research, designed the study, read the HRCT examinations and wrote the manuscript; De Carli M contributed to designing the study and writing the manuscript; d'Angelo P and Zanelli E collected the data and contributed to analysing the data and writing the manuscript; Zuiani C drafted the concept of the research and contributed to designing the study; Girometti R designed the study, analysed the data and contributed to writing the manuscript.

Institutional review board statement: Our referring Ethical Committee approved this study.

Conflict-of-interest statement: All authors declare no conflicts of interest related to this article.

Lorenzo Cereser, Paola d'Angelo, Elisa Zanelli, Chiara Zuiani, Rossano Girometti, Institute of Radiology, Department of Medicine, University of Udine, Azienda Sanitaria Universitaria Integrata di Udine, Udine 33100, Italy

Marco De Carli, Second Unit of Internal Medicine, Azienda Sanitaria Universitaria Integrata di Udine, Udine 33100, Italy

Paola d'Angelo, Department of Imaging, Bambino Gesù Chlidren's Hospital, IRCCS, Rome 00165, Italy

Abstract

AIM

To compare high-resolution computed tomography (HRCT) findings between humoral primary immunodeficiencies (hPIDs) subtypes; to correlate these findings to pulmonary function tests (PFTs).

METHODS

We retrospectively identified 52 consecutive adult patients with hPIDs who underwent 64-row HRCT and PFTs at the time of diagnosis. On a per-patient basis, an experienced radiologist recorded airway abnormalities (bronchiectasis, airway wall thickening, mucus plugging, tree-in-bud, and air-trapping) and parenchymal-interstitial abnormalities (consolidations, ground-glass opacities, linear and/or irregular opacities, nodules, and bullae/cysts) found on HRCT. The chi-square test was performed to compare the prevalence of each abnormality among patients with different subtypes of hPIDs. Overall logistic regression analysis was performed to assess whether HRCT findings predicted obstructive and/or restrictive PFTs results (absent-to-mild *vs* moderate-to-severe).

RESULTS

Thirty-eight of the 52 patients with hPIDs showed common variable immunodeficiency disorders (CVID), while the remaining 14 had CVID-like conditions (*i.e.*, 11 had isolated IgG subclass deficiencies and 3 had selective IgA deficiencies). The prevalence of most HRCT abnormalities was not significantly different between CVID and CVID-like patients ($P > 0.05$), except for linear and/or irregular opacities (prevalence of 31.6% in the CVID group and 0 in the CVID-like group; $P = 0.0427$). Airway wall thickening was the most frequent HRCT abnormality found in both CVID and CVID-like patients (71% of cases in both groups). The presence of tree-in-bud abnormalities was an independent predictor of moderate-to-severe obstructive defects at PFTs (Odds Ratio, OR, of

Manuscript source: Unsolicited manuscript

Correspondence to: Lorenzo Cereser, MD, Doctor, Institute of Radiology, Department of Medicine, University of Udine, Azienda Sanitaria Universitaria Integrata di Udine, p.le S. Maria della Misericordia 15, Udine 33100, Italy. lcereser@sirm.org
Telephone: +39-432-559266
Fax: +39-432-559867

Received: July 17, 2018
Peer-review started: July 17, 2018
First decision: August 8, 2018
Revised: September 22, 2018
Accepted: October 7, 2018
Article in press: October 7, 2018
Published online: November 28, 2018

18.75, $P < 0.05$), while the presence of linear and/or irregular opacities was an independent predictor of restrictive defects at PFTs (OR = 13.00; $P < 0.05$).

CONCLUSION
CVID and CVID-like patients showed similar HRCT findings. Tree-in-bud and linear and/or irregular opacities predicted higher risks of, respectively, obstructive and restrictive defects at PFTs.

Key words: Bronchiectasis; Multidetector computed tomography; Common variable immunodeficiency; Immunologic deficiency syndromes; Respiratory function tests

Core tip: Humoral primary immunodeficiencies (hPIDs) are a group of conditions characterized by impaired antibody production and presenting with recurrent respiratory infections, autoimmune diseases, and malignancy. Chest high-resolution computed tomography (HRCT) is the imaging technique of choice for detecting, characterizing, and quantifying lung complications in these patients. The aims of this study were to compare HRCT findings in 52 patients with hPIDs subtypes (common variable immunodeficiency disorders - CVID *vs* CVID-like), and evaluate whether these findings may predict pulmonary function tests results. CVID *vs* CVID-like patients showed comparable HRCT findings. The presence of tree-in-bud and linear and/or irregular opacities were independent predictors of, respectively, significant obstructive and restrictive defects.

Cereser L, De Carli M, d'Angelo P, Zanelli E, Zuiani C, Girometti R. High-resolution computed tomography findings in humoral primary immunodeficiencies and correlation with pulmonary function tests. *World J Radiol* 2018; 10(11): 172-183
URL: https://www.wjgnet.com/1949-8470/full/v10/i11/172.htm
DOI: https://dx.doi.org/10.4329/wjr.v10.i11.172

INTRODUCTION

Humoral primary immunodeficiencies (hPIDs), also known as primary predominantly antibody deficiencies, constitute the most common subgroup of primary immunodeficiency disorders (about 50% of diagnoses)[1]. hPIDs encompass a spectrum of conditions characterized by impaired antibody production, manifesting with recurrent respiratory tract infections, increased susceptibility to autoimmune diseases, and malignancy[1,2]. Common variable immunodeficiency disorders (CVID) are the most clinically significant group of hPIDs (with a prevalence of about 1:25000-1:50000 subjects). These disorders show distinct clinical and laboratory phenotypes associated with low levels of IgG and IgA and/or IgM[3,4]. CVID onset is during adult life in 70% of the cases, generally occurring between 20 and 40 years of age[5,6]. Other hPIDs are often referred as "CVID-like" conditions: these conditions are in most cases asymptomatic and include selective IgA deficiency (the most frequent hPID, with a prevalence of 1/600 in white people) and isolated IgG subclass deficiency[2,7,8].

Overall, thoracic complications develop in 60% of patients with hPIDs, representing the leading cause of morbidity and mortality. Chest high-resolution computed tomography (HRCT) is the imaging technique of choice for detecting, characterizing, and quantifying lung complications, as well as for evaluating the response to therapy[1,9,10]. It is generally accepted that the initial evaluation of newly diagnosed patients should include HRCT and pulmonary function tests (PFTs). Early identification of respiratory complications provides a baseline assessment of lung involvement, allows prompt treatment to reduce the number of pulmonary infections, and impacts on quality of life and mortality, the latter being influenced by both structural and functional pulmonary impairment[5,11,12].

Several studies have reported HRCT findings in hPIDs; these findings include non-infective airway disorders (*i.e.*, bronchiectasis, airway wall thickening, and air trapping), pulmonary infections, diffuse lung parenchymal diseases [*e.g.*, Granulomatous and Lymphocytic Interstitial Lung Disease (GLILD), and organising pneumonia], and thoracic neoplasms (*e.g.*, lymphoma)[10,13-16]. However, most papers

refer only to CVID patients, and report that HRCT abnormalities are present in more than 90% of those patients[9,17]. While some Authors reported that the severity of HRCT abnormalities was not significantly different between CVID and CVID-like paediatric patients[18,19], to the best of our knowledge no studies have addressed this issue in adult patients. Demonstrating a difference between CVID and CVID-like patients may influence the time intervals between HRCT examinations during follow-up in these 2 subgroups of hPIDs. In addition to this, previous studies assessing a correlation between HRCT findings and PFTs results demonstrated contradictory results[9,17,18,20].

The purpose of this study was twofold: (1) to compare HRCT pulmonary findings in adult patients among different subgroups of hPIDs (*i.e.*, CVID and CVID-like); and (2) to assess whether HRCT findings predict PFTs results.

MATERIALS AND METHODS

Study population and PFTs

Our referring Ethical Committee approved this study. The need for informed consent was waived due to the retrospective design of the study. By performing a computerized search, we identified 56 adult patients who received a definite diagnosis of hPIDs, in accordance with the European Society for Immunodeficiencies criteria[21], in our tertiary referral centre and between 2012 and 2016. Diagnosis was performed after a history of previously undefined respiratory disease ranging from 1 to 5 years in duration. All patients underwent HRCT and PFTs within one month from diagnosis as a part of the diagnostic workflow performed at our institute. Accordingly, hereinafter we are going to refer to the HRCT performed at the time of diagnosis as baseline HRCT. Four patients were excluded from the study due to infectious respiratory disease at the time of HRCT (clinically unstable disease) or unavailability of the PFTs results. Therefore, the final population included 52 patients and had the following distribution of disease subtypes: 38 CVID, 11 isolated IgG subclass deficiency, and 3 selective IgA deficiency cases.

Lung function was evaluated according to the criteria of the European Respiratory Society/American Thoracic Society task force[22]. The following parameters were measured with a spirometer (Vmax 29c; Sensor Medics, Yorba Linda, CA, United States): Forced expiratory volume in one second (FEV1), forced vital capacity (FVC), vital capacity (VC), peak expiratory flow (PEF), and total lung capacity (TLC). Obstructive ventilatory defects were diagnosed when the reduced FEV1/VC ratio was below the 5th percentile of the predicted value; restrictive ventilatory disorders were diagnosed when a reduction in TLC below the 5th percentile of the predicted value was detected in the presence of a normal FEV1/VC ratio. The severity of ventilatory defects was assessed using a six-point scale (absent, mild, moderate, moderately severe, severe, and very severe)[23]. For the purposes of analysis, patients with obstructive or restrictive defects were classified in two groups: (1) patients with absent-to-mild defects (*i.e.*, ≥ 70% of predicted values); and (2) patients with moderate-to-severe defects (*i.e.*, < 70% of predicted values).

HRCT examinations

HRCT examinations were performed with a 64-row MDCT scanner (Discovery HD 750, GE Healthcare, Milwaukee, WI, United States), with the patient in the supine position. The whole thorax was scanned volumetrically at suspended full inspiration using the following acquisition parameters: tube potential, 120 kV; tube current modulation range, 150-400 mA (based on a Noise Index set at 18.4); rotation time, 0.8 s; detector configuration, 64 mm × 0.625 mm; reconstructed section thickness and reconstructed interval, 1.25 mm; field of view according to patient size. In 32/52 patients an additional end-expiratory volumetric scan with the same parameters was also acquired.

Images were reconstructed using a high-spatial-frequency algorithm, and displayed with lung parenchyma (level, -500 HU; width, 1500 HU) and mediastinum windowing (level, 50 HU; width, 350 HU).

Image analysis

A radiologist with 8 years of experience in pulmonary imaging, blinded to patient history and lung function, reviewed the HRCT examinations on a picture archiving and communication system workstation (Suitestensa Ebit srl, Esaote Group Company, Genoa, Italy). Post-processing techniques, including Multiplanar Reconstruction (MPR), Maximum Intensity Projection (MIP) and Minimum Intensity Projection (MinIP), were available to complement the analysis of thin source images.

For each patient, the reader recorded two classes of abnormalities: airway abnormalities (*i.e.*, airway wall thickening, tree-in-bud, bronchiectasis, mucus plugging, and air trapping), and parenchymal-interstitial abnormalities (*i.e.*, linear and/or irregular opacities, nodules, consolidations, ground-glass opacities, and bullae/cysts). Radiological features were evaluated according to the Fleischner Society glossary[24]. In particular, "linear and/or irregular opacities" describe any linear opacity of irregular thickness that does not respect the lung architecture[9] and has been reported as being a key feature of lung disease in CVID patients.

Any individual abnormality was scored using a double three-point scale (with a total score ranging from 2 to 6), for coding two aspects simultaneously: (1) extension, with 1 = involvement of a single pulmonary lobe, 2 = two-to-three lobes involved, 3 = more than three lobes involved; and (2) conspicuity in the most involved lobe, with 1 = mild, 2 = moderate, and 3 = severe. As to include in the analysis only findings that are reasonably related to hPIDs, the minimum required total score for an abnormality was 3.

Statistical analysis

We calculated the per-patient prevalence of each of the aforementioned HRCT abnormalities in the overall population and in different subgroups of hPIDs patients, *i.e.*, the CVID group *vs* CVID-like group (the latter including both isolated IgG subclass deficiencies and selective IgA deficiencies). Main clinical features (age, duration of symptoms before definite diagnosis, and ventilatory defects) and prevalence of HRCT abnormalities were compared between the two groups using, respectively, the *u*-Mann-Whitney and χ^2 tests. A logistic regression analysis (stepwise approach) was performed to assess whether the HRCT findings could predict a significant obstructive or restrictive defect at PFTs on the overall study population. As variables we used each of the aforementioned airway abnormalities and parenchymal-interstitial abnormalities. Obstructive and restrictive defects were defined as relevant only if they were of moderate-to-severe nature, and not if they were absent-to-mild. Air trapping was excluded from the model since HRCT additional expiratory scan was not available for all patients. Analysis was performed with a commercially available software (MedCalc version 12.5.0.0, MariaKerke, Belgium). The α level was set to 0.05.

RESULTS

Study population and PFTs results

Of the 52 hPIDs patients 37 were females and 15 were males, with a mean age of 53.9 ± 12.7 years. Thirty-eight of the 52 patients (73%) were included in the CVID group, and 14/52 patients (27%) were in the CVID-like group. No significant differences between the two groups were found in terms of age (mean 54.9 ± 12.9 years in the CVID group *vs* 51 ± 11.9 years in the CVID-like group) and average duration of symptoms before definite diagnosis of hPIDs (2 years, range 1-3, in the CVID group *vs* 4 years, range 1-5, in the CVID-like group, $P > 0.05$). None of the patients underwent HRCT before hPIDs diagnosis. Standard CTs were available for 15 of the 52 patients (one examination each) and had been performed 2-4 years before the HRCT at the time of hPIDs diagnosis.

The results of the PFTs show that almost half of the patients (25/52, 48.1%) had ventilatory defects (Table 1). Three patients in the CVID group had concomitant moderate-to-severe obstructive defects and restrictive defects. None of the patients in the CVID-like group showed restrictive defects. No statistically significant differences were found between the two subgroups of hPIDs in terms of prevalence of obstructive (CVID: 44.7% *vs* CVID-like: 42.9%, $P = 0.8474$) and restrictive defects (CVID: 13.1% *vs* CVID-like: 0%, $P = 0.2052$).

Distribution of HRCT abnormalities in the study groups

We recorded a high prevalence of HRCT findings, with one or more abnormalities detected in 47/52 hPIDs patients (90.4%). The prevalence of specific airway abnormalities was not significantly different between the CVID and CVID-like groups ($P > 0.05$, Table 2). Airway wall thickening was the most commonly found abnormality and showed a comparable prevalence in both groups (71.0% in the CVID group and 71.4% in the CVID-like group, Figure 1).

Regarding HRCT parenchymal-interstitial abnormalities, linear and/or irregular opacities were present in 31.6% of the patients in the CVID group and in none of those in the CVID-like group, with borderline significance ($P = 0.0427$, Table 2). Nodules were the most frequent finding in both groups, with a prevalence of 50.0% (Figure 2).

Table 1 Pulmonary function tests results *n* (%)

	Obstructive defect				Restrictive defect			
	Absent	Mild	Significant[1]	Any	Absent	Mild	Significant[1]	Any
CVID (n = 38)	21 (55.3)	10 (26.3)	7 (18.4)	17 (44.7)	33 (86.9)	1 (2.6)	4 (10.5)	5 (13.1)
CVID-like (n = 14)	8 (57.1)	2 (14.3)	4 (28.6)	6 (42.9)	14 (100)	0 (0)	0 (0)	0 (0)
All patients (n = 52)	29 (55.8)	12 (23.1)	11 (21.2)	23 (44.2)	47 (90.4)	1 (1.9)	4 (7.7)	5 (9.6)

Data are presented as number of patients with percentages in parentheses.
[1]Moderate-to-severe defect. CVID: Common variable immunodeficiency disorder; CVID-like: Including isolated IgG subclass deficiency and selective IgA deficiency.

Correlation between HRCT abnormalities and PFTs

The distributions of HRCT-detected airway and parenchymal-interstitial abnormalities according to severity of ventilatory defects assessed at PFTs are reported in Tables 3 and 4.

Regarding HRCT-detected airway abnormalities, both mucus plugging (P = 0.0112, Figure 3) and tree-in-bud (P = 0.0014, Figure 4) were found to be significantly associated with a relevant obstructive defect assessed at PFTs. However, on multivariate analysis, tree-in-bud was the only independent predictor (P = 0.0027) of relevant obstructive defect, with an odds ratio (OR) of 18.75 (95%CI: 2.76-127.52).

Additionally, regarding HRCT-detected parenchymal-interstitial abnormalities, the presence of linear and/or irregular opacities (Figure 5) was the only predictor of relevant restrictive defect both at univariate (P = 0.0029) and multivariate analysis (P = 0.0344; OR, 13.00; 95%CI: 1.21-139.97).

DISCUSSION

Pulmonary abnormalities in hPIDs adult patients were common in our series: Only 9.6% of our patients had negative HRCTs at the time of diagnosis, a finding in agreement with the literature (range 4%-17%)[9,17,25]. The prevalence of most of airways and parenchymal-interstitial findings was not significantly different between the CVID and the CVID-like groups. Similarly, PFTs results were comparable between the two subtypes of hPIDs, showing a larger prevalence of obstructive defects (45% in the CVID group and 43% in the CVID-like group) over restrictive defects (13% in the CVID group and 0 in the CVID-like group). These findings are in agreement with the previously reported prevalences in CVID patients (9%-53% for obstructive defects and 5%-34% for restrictive defects)[9,17,26,27]. Conversely, to the best of our knowledge, this is the first study reporting prevalences in adult CVID-like patients. Overall, our findings support the hypothesis that neither imaging nor PFTs can reliably differentiate between the two groups of CVID and CVID-like patients. One might argue that the relevance of this result is impaired by the relatively small population included in the present study. However, our series reflects the rarity of both conditions, and is one of the largest published reports on HRCT as far as we know.

Of note, linear and/or irregular opacities were more frequently found in CVID patients (32%) than in CVID-like patients (0), although statistical significance was borderline (P = 0.0427). Gregersen *et al*[9] highlighted the importance of this abnormality in CVID adult patients, both because of its frequency (about 52% of cases) and its close association with impaired gas diffusion. In line with the relevant literature[11,28], we found that only one HRCT abnormality, linear and/or irregular opacities, was a predictor of significant restrictive defects. This result emphasizes the importance of prompt identification of this abnormality at baseline evaluation. Overall, our results support the assumption that CVID-like patients are clinically and immunologically comparable to CVID patients[18,29], although the latter show more frequently radiological abnormalities associated to interstitial disease (*i.e.*, linear and/or irregular opacities).

It is likely that the prevalence of different HRCT findings might reflect the effects of the specific disease on the lungs in CVID and CVID-like patients. The most frequent findings in our cohort were bronchiectasis (69.2%) and airway wall thickening (71.2%, Figure 2), and are in line with those previously reported in adult patients (range 40%-70% for bronchiectasis and 68%-75% for airway wall thickening)[9,10,17,25,26]. Such a high prevalence can be explained by the cumulative effect of respiratory tract infections[17,30,31]. Other common findings in our study were nodules (found in 50% of

Figure 1 Airway wall thickening. A 65-year-old male patient with common variable immunodeficiency disorder. High-resolution computed tomography shows diffuse airway wall thickening in the right middle and lower lobes (straight arrows); centrilobular and tree-in-bud nodules in the right lung are also detected (curved arrow).

patients *vs* 29%-55% reported in literature)[9,17,25] and mucus plugging (in 44.2% of patients). We did not differentiate among various types of nodules, since their characteristics reflect a wide spectrum of conditions (including infectious diseases, previous infections or lymphoproliferative and/or granulomatous conditions) that cannot be histologically confirmed in most patients[14,25]. We believe that the high prevalence of nodules should be considered as an epiphenomenon of other coexisting pulmonary abnormalities rather than a definite hallmark of CVID or CVID-like hPIDs. However, the finding of mucus plugging mirrors more specifically the inflammation of large airways[9], with a reported prevalence in hPIDs ranging between 25% and 35%[9,17]. Last, air trapping was frequent (50%) in the subgroup of patients for whom an expiratory scan was available. Although incomplete, the prevalence we describe is in the range of those previously reported in CVID patients (45%-63%)[9,17,25].

Concerning the less frequent HRCT findings, we detected tree-in-bud abnormalities in 19% of the patients, similarly to what reported by Tanaka *et al*[25] (20%) in a study assessing a CVID population. This sign reflects a spectrum of both endobronchiolar and peribronchiolar disorders[24]. The main causes of tree-in-bud findings in the general population are reported to be acute or chronic infections mainly from nontuberculous mycobacteria and bacteria (*e.g.*, *Staphylococcus aureus* and *Pseudomonas aeruginosa*)[32,33]. Previous studies demonstrated the presence of potentially pathogenic bacteria (and viruses) in the lungs of patients with clinically stable hPIDs[34]. In our series, most of the tree-in-bud cases were of infectious origin, albeit asymptomatic, at the time of HRCT. The majority of these patients (80%) showed coexisting bronchiectasis, a major predisposing factor for infections[32]. Follicular bronchiolitis (FB) is another cause of tree-in-bud sign detected at HRCT[35,36]. FB is a reactive pulmonary lymphoid disorder reported in CVID patients, is presumably related to recurrent pneumonia, and is characterized by the development of lymphoid follicles and germinal centres with peribronchial/peribronchiolar distribution[37]. In our population, 2 of the 10 cases with tree-in-bud abnormalities were CVID patients who developed GLILD, a condition in which FB is a typical finding[38,39]. In addition, consolidation was found in 27% of our study population (*vs* 17%-64% reported in the literature) and ground-glass opacities in 25% of the patients (*vs* 12%-34% in the literature)[9,10,17,25]. Although the nature of most of these abnormalities remained undetermined, it is likely that they represent the effects of subclinical or previous infections, thus not requiring specific radiological work-up in the absence of clinical suspicion of lymphoma or cancer.

In patients with CVID, HRCT was proven to detect silent progression earlier than PFTs, because of its capability to assess even subtle structural abnormalities[34,40]. Not surprisingly, alterations detected by PFTs are less frequent than those detected by HRCT[40], an observation confirmed in our study that also includes CVID-like patients (prevalence was 48.1% by PFTs *vs* 90.4% by HRCT). This observation raises some questions on how to follow up the patient after baseline evaluation. Current recommendations suggest PFTs intervals of 6-12 mo, and HRCT intervals ranging from 1 to 5 years[11,17]. By multivariate analysis, we found that detection of tree-in-bud abnormalities predicts obstructive defects (OR 18.75), and detection of linear and/or irregular opacities predicts restrictive defects (OR 13.00). By contrast, none of the other, more frequent findings were independent predictors of obstructive or restrictive defects. This observation supports previous data on CVID showing a moderate correlation between PFTs and HRCT results, as well as the idea that these

Table 2 Prevalence of high-resolution computed tomography-detected abnormalities in the two humoral primary immunodeficiencies subtypes (CVID and CVID-like), and comparison between the two groups *n* (%)

Abnormality	All patients *n* = 52	CVID *n* = 38	CVID-like *n* = 14	*P*-value (CVID *vs* CVID-like)
Airway abnormalities				
Bronchiectasis	36 (69.2)	27 (71)	9 (64.3)	0.8964
Airway wall thickening	37 (71.2)	27 (71)	10 (71.4)	0.7501
Tree-in-bud	10 (19.2)	6 (15.8)	4 (28.6)	0.8464
Mucus plugging	23 (44.2)	16 (42.1)	7 (50)	0.8888
Air trapping[1]	16 (50)	12 (52.2)	4 (44.4)	0.8557
Parenchymal-interstitial abnormalities				
Consolidation	14 (26.9)	11 (28.9)	3 (21.4)	0.8495
Ground-glass opacity	13 (25)	12 (31.6)	1 (7.1)	0.1487
Nodules	26 (50)	19 (50)	7 (50)	1
Linear and/or irregular opacities	12 (23.1)	12 (31.6)	0 (0)[a]	0.0427
Bullae/cysts	5 (9.6)	5 (13.2)	0 (0)	0.3695

[a]P <0.05.
[1]Values are calculated on the 32 patients (23 CVID + 9 CVID-like) for whom additional expiratory scan was acquired. Chi-square test: CVID *vs* CVID-like patients; CVID: Common variable immunodeficiency disorders; CVID-like: Including isolated IgG subclass deficiency and selective IgA deficiency.

two examinations assess different aspects of the disease[40]. Of note, Maarschalk-Ellerbroek *et al*[17] found a poor correlation between detection of tree-in-bud abnormalities and PFTs. However, these authors evaluated tree-in-bud abnormalities in a combined score with mucus plugging, which impairs a direct comparison with our findings. Our results suggest that morphological assessment with HCRT might be postponed as much as possible to maximize cost-effectiveness and reduce radiation exposure. A possible exception to this might be the case of patients showing tree-in-bud or linear and/or irregular opacities: scheduling HRCTs at shorter intervals for these patients might provide a reliable morphological counterpart of pulmonary function. Our hypothesis is extrapolated from the observation of baseline examinations in our population; therefore, further studies with a more specific purpose and a prospective design should be performed to confirm this statement.

We acknowledge that our study has some limitations. First, an HRCT supplementary expiratory scan was not available in 38% of the patients because of the retrospective nature of the study. Hence, we were not able to include air trapping as a variable in the logistic regression analysis to predict PFTs results. Previous studies found a significant correlation between air trapping and airway obstruction both in children and in adult patients with CVID[9,20]. While we acknowledge that we should have included air trapping to study both CVID and CVID-like groups, we believe that most of the relevant HRCT findings support our conclusions. Second, we did not consider the extent and/or distribution of individual HRCT findings in the prediction analysis of PFTs results. The use of dedicated HRCT scoring systems, which were originally developed for CVID patients and/or for paediatric populations only, could help studying this issue also in adult patients with CVID and CVID-like conditions[9,17,18,20]. Third, we were not able to assess the radiologic evolution of the disease over time because of the lack of previous HRCTs, which could have been used for a comparison with the baseline HRCT. However, our study actually reflects the clinical reality, in which a delay between the onset of respiratory infections-related symptoms and the definite diagnosis of hPIDs is common (median of 8 years in adults aged over 30 years old, according to The United Kingdom Primary Immunodeficiency Registry)[41]. In this scenario, the first HRCT is frequently performed only at the time of diagnosis.

In conclusion, we found no significant difference in the prevalence of most of HRCT findings or PFTs abnormalities between CVID and CVID-like conditions. Our results support the hypothesis that these two conditions are comparable hPIDs subtypes and candidate to similar management. The detection of tree-in-bud abnormalities was found to be an independent predictor of obstructive defects assessed at PFTs, while the detection of linear and/or irregular opacities was an independent predictor of restrictive defects assessed at PFTs. Our observations suggest that patients showing these findings might benefit from more frequent HRCTs during follow-up as to evaluate the morphological abnormalities associated with their function impairment.

Table 3 Distribution of high-resolution computed tomography-detected airway abnormalities according to the severity of obstructive defect at pulmonary function tests in the overall study population, and results of logistic regression analysis for prediction of moderate-to-severe obstructive defects at PFTs *n* (%)

Abnormality	Absent	Mild	Moderate	Severe	Univariate analysis	Multivariate analysis
	n = 29	*n* = 12	*n* = 9	*n* = 2	*P*-value	*P*-value (odds ratio)
Bronchiectasis	19 (66.5)	9 (75)	7 (77.8)	1 (50)	NS	NS
Airway wall thickening	20 (69)	9 (75)	6 (66.7)	2 (100)	NS	NS
Tree-in-bud	2 (6.9)	2 (16.7)	5 (55.6)	1 (50)	0.0014	0.0027 (18.75)
Mucus plugging	8 (27.6)	8 (66.7)	5 (55.6)	2 (100)	0.0112	NS

NS: Non-significant.

Table 4 Distribution of high-resolution computed tomography-detected parenchymal-interstitial abnormalities according to the severity of the restrictive defects at pulmonary function tests in the overall study population, and results of logistic regression analysis for prediction of moderate-to-severe restrictive defects at PFTs *n* (%)

Abnormality	Absent	Mild	Moderate	Severe	Univariate analysis	Multivariate analysis
	n = 47	*n* = 1	*n* = 4	*n* = 0	*P*-value	*P*-value (odds ratio)
Consolidation	11 (23.4)	1 (100)	2 (50)	0 (0)	NS	NS
Ground-glass opacity	10 (21.3)	1 (100)	2 (50)	0 (0)	NS	NS
Nodules	23 (48.9)	1 (100)	2 (50)	0 (0)	NS	NS
Linear and/or irregular opacities	8 (17)	1 (100)	3 (75)	0 (0)	0.0029	0.0344
Bullae/cysts	5 (10.6)	0 (0)	0 (0)	0 (0)	NS	NS

NS: Non-significant.

Figure 2 Nodules. A 64-year-old female patient with common variable immunodeficiency disorder. High-resolution computed tomography shows multiple, small nodules with peribronchial and perifissural location in the upper and lower lobes of both lungs (arrows). A diagnosis of granulomatous and lymphocytic interstitial lung disease was subsequently made.

Figure 3 Mucus plugging. A 65-year-old male patient with common variable immunodeficiency disorder. Para-coronal 2-mm minimum intensity projection high-resolution computed tomography image shows mild bronchiectasis with extensive mucus plugging in the left lower lobe (arrow).

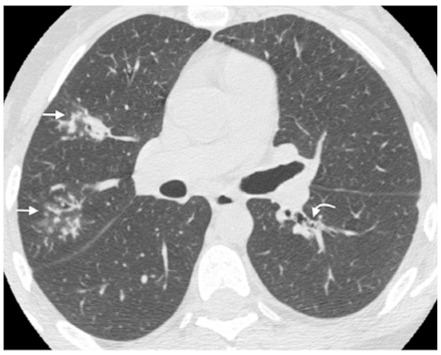

Figure 4 Tree-in-bud. A 40-year-old female patient with isolated IgG2 subclass deficiency. High-resolution computed tomography shows centrilobular and tree-in-bud nodules in the right upper lobe (straight arrows); small mucus plugging in the left lower lobe is also detected (curved arrow).

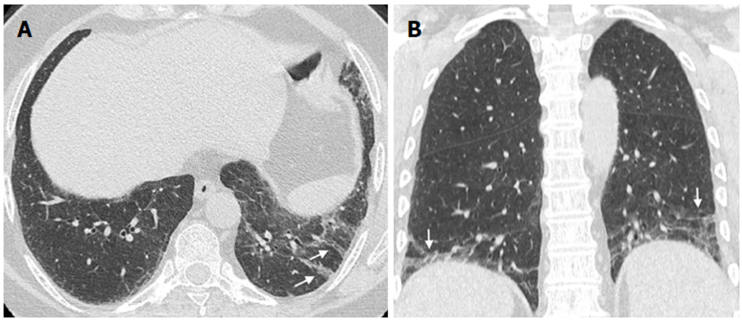

Figure 5 Linear and/or irregular opacities. A 66-year-old female patient with common variable immunodeficiency disorder. A: High-resolution computed tomography shows patchy areas of ground-glass opacity, along with reticulation and linear and/or irregular opacities (arrows) in both lower lobes; B: Coronal reformatted image shows the peripheral and basal-predominant distribution of the findings (arrows).

ARTICLE HIGHLIGHTS

Research background

Common variable immunodeficiency disorders (CVID) are the most clinically significant group of humoral primary immunodeficiency diseases (hPIDs), manifesting with recurrent respiratory tract infections and increased susceptibility to autoimmune diseases and malignancy. Other hPIDs are often termed "CVID-like" conditions, and include selective IgA deficiency and isolated IgG subclass deficiency. The initial evaluation of patients newly diagnosed with hPIDs should include high-resolution computed tomography (HRCT) and pulmonary function tests (PFTs).

Research motivation
To the best of our knowledge no previous studies assessed whether HRCT findings differ in terms of prevalence among the two subtypes of hPIDs in adult patients. Demonstrating a difference between CVID and CVID-like patients may influence the time intervals between HRCT examinations during follow-up in these 2 subgroups of hPIDs. Moreover, previous studies assessing a possible correlation between HRCT findings and PFTs results demonstrated contradictory results.

Research objectives
The purpose of this study was twofold: (1) to compare HRCT pulmonary findings in adult patients with different subgroups of hPIDs (*i.e.*, CVID *vs* CVID-like); and (2) to assess whether HRCT findings predict PFTs results.

Research methods
We included 52 adult patients (38 CVID and 14 CVID-like) who received a definite diagnosis of hPIDs and underwent HRCT and PFTs within one month from the time of diagnosis. One pulmonary radiologist, blinded to patient history and lung function: (1) reviewed the HRCT examinations; (2) recorded two classes of abnormalities, namely airway abnormalities and/or parenchymal-interstitial abnormalities; and (3) scored all abnormalities according to their extension and conspicuity. We calculated the per-patient prevalence of each HRCT abnormality in the overall population and in both subgroups of hPIDs patients, (CVID and CVID-like groups). We performed a logistic regression analysis to assess whether HRCT findings were predictive of a relevant obstructive or restrictive defect at PFTs on the overall study population.

Research results
Of the 52 hPIDs patients, 37 were females and 15 were males, with a mean age of 53.9 ± 12.7 years. We found a high prevalence of HRCT findings (90.4% patients had one or more abnormalities). The prevalence of each of the airway abnormalities considered was not significantly different between the CVID and CVID-like group. Regarding HRCT-detected parenchymal-interstitial abnormalities, the only relevant result was the finding of linear and/or irregular opacities, showing a prevalence of 31.6% in the CVID group and 0 in the CVID-like group, with borderline significance. The presence of tree-in-bud abnormalities was an independent predictor of obstructive defects at PFTs (Odds Ratio, OR, of 18.75, $P < 0.05$), while the presence of linear and/or irregular opacities was an independent predictor of restrictive defects at PFTs (OR = 13.00; $P < 0.05$).

Research conclusions
No previous research compared the prevalence of HRCT findings in different subtypes of hPIDs adult patients. After dividing hPIDs patients in CVID *vs* CVID-like groups, we observed no significant difference in the prevalence of most of airways and parenchymal-interstitial findings between the two groups. This observation supports the hypothesis that these two groups represent comparable hPIDs subtypes, and are candidate to similar management. Tree-in-bud and linear and/or irregular opacities were found to be independent predictors of, respectively, obstructive and restrictive defects on PFTs.

Research perspectives
Our results suggest that morphological assessment with HRCT might be delayed as much as possible to maximize cost-effectiveness and reduce radiation exposure. A possible exception to this might be the case of patients showing tree-in-bud or linear and/or irregular opacities: Scheduling HRCTs at shorter intervals for these patients might provide a reliable morphological counterpart of pulmonary function. Further prospective studies with a proper design are needed to confirm this hypothesis in the follow-up period.

ACKNOWLEDGMENTS

The authors thank Viviana Moroso of MV Medical Writing (Lulea, Sweden) for copyediting the manuscript, a service that was funded by Department of Medicine, University of Udine (Udine, Italy) in accordance with Good Publication Practice (GPP3) guidelines (http://www.ismpp.org/gpp3).

REFERENCES

1 **Bonilla FA**, Khan DA, Ballas ZK, Chinen J, Frank MM, Hsu JT, Keller M, Kobrynski LJ, Komarow HD, Mazer B. Practice parameter for the diagnosis and management of primary immunodeficiency. *J Allergy Clin Immunol* 2015; **136**: 1186-1205.e1-78 [PMID: 26371839 DOI: 10.1016/j.jaci.2015.04.049]
2 **Notarangelo LD**. Primary immunodeficiencies. *J Allergy Clin Immunol* 2010; **125**: S182-S194 [PMID: 20042228 DOI: 10.1016/j.jaci.2009.07.053]
3 Primary immunodeficiency diseases. Report of an IUIS Scientific Committee. International Union of Immunological Societies. *Clin Exp Immunol* 1999; **118** Suppl 1: 1-28 [PMID: 10540200 DOI: 10.1046/j.1365-2249.1999.00109.x]
4 **Picard C**, Bobby Gaspar H, Al-Herz W, Bousfiha A, Casanova JL, Chatila T, Crow YJ,

Cunningham-Rundles C, Etzioni A, Franco JL. International Union of Immunological Societies: 2017 Primary Immunodeficiency Diseases Committee Report on Inborn Errors of Immunity. *J Clin Immunol* 2018; **38**: 96-128 [PMID: 29226302 DOI: 10.1007/s10875-017-0464-9]

5 **Resnick ES**, Moshier EL, Godbold JH, Cunningham-Rundles C. Morbidity and mortality in common variable immune deficiency over 4 decades. *Blood* 2012; **119**: 1650-1657 [PMID: 22180439 DOI: 10.1182/blood-2011-09-377945]

6 **Tam JS**, Routes JM. Common variable immunodeficiency. *Am J Rhinol Allergy* 2013; **27**: 260-265 [PMID: 23883805 DOI: 10.2500/ajra.2013.27.3899]

7 **Janzi M**, Kull I, Sjöberg R, Wan J, Melén E, Bayat N, Ostblom E, Pan-Hammarström Q, Nilsson P, Hammarström L. Selective IgA deficiency in early life: association to infections and allergic diseases during childhood. *Clin Immunol* 2009; **133**: 78-85 [PMID: 19541543 DOI: 10.1016/j.clim.2009.05.014]

8 **Palmer DS**, O'Toole J, Montreuil T, Scalia V, Yi QL, Goldman M, Towns D. Screening of Canadian Blood Services donors for severe immunoglobulin A deficiency. *Transfusion* 2010; **50**: 1524-1531 [PMID: 20158683 DOI: 10.1111/j.1537-2995.2010.02588.x]

9 **Gregersen S**, Aaløkken TM, Mynarek G, Kongerud J, Aukrust P, Frøland SS, Johansen B. High resolution computed tomography and pulmonary function in common variable immunodeficiency. *Respir Med* 2009; **103**: 873-880 [PMID: 19181508 DOI: 10.1016/j.rmed.2008.12.015]

10 **Bondioni MP**, Duse M, Plebani A, Soresina A, Notarangelo LD, Berlucchi M, Grazioli L. Pulmonary and sinusal changes in 45 patients with primary immunodeficiencies: computed tomography evaluation. *J Comput Assist Tomogr* 2007; **31**: 620-628 [PMID: 17882044 DOI: 10.1097/RCT.0b013e31802e3c11]

11 **Verma N**, Grimbacher B, Hurst JR. Lung disease in primary antibody deficiency. *Lancet Respir Med* 2015; **3**: 651-660 [PMID: 26188881 DOI: 10.1016/S2213-2600(15)00202-7]

12 **Hurst JR**, Workman S, Garcha DS, Seneviratne SL, Haddock JA, Grimbacher B. Activity, severity and impact of respiratory disease in primary antibody deficiency syndromes. *J Clin Immunol* 2014; **34**: 68-75 [PMID: 24136152 DOI: 10.1007/s10875-013-9942-x]

13 **Bierry G**, Boileau J, Barnig C, Gasser B, Korganow AS, Buy X, Jeung MY, Roy C, Gangi A. Thoracic manifestations of primary humoral immunodeficiency: a comprehensive review. *Radiographics* 2009; **29**: 1909-1920 [PMID: 19926753 DOI: 10.1148/rg.297095717]

14 **Hampson FA**, Chandra A, Screaton NJ, Condliffe A, Kumararatne DS, Exley AR, Babar JL. Respiratory disease in common variable immunodeficiency and other primary immunodeficiency disorders. *Clin Radiol* 2012; **67**: 587-595 [PMID: 22226567 DOI: 10.1016/j.crad.2011.10.028]

15 **Cereser L**, Girometti R, d'Angelo P, De Carli M, De Pellegrin A, Zuiani C. Humoral primary immunodeficiency diseases: clinical overview and chest high-resolution computed tomography (HRCT) features in the adult population. *Clin Radiol* 2017; **72**: 534-542 [PMID: 28433201 DOI: 10.1016/j.crad.2017.03.018]

16 **Bang TJ**, Richards JC, Olson AL, Groshong SD, Gelfand EW, Lynch DA. Pulmonary Manifestations of Common Variable Immunodeficiency. *J Thorac Imaging* 2018; **33**: 377-383 [PMID: 30067570 DOI: 10.1097/RTI.0000000000000350]

17 **Maarschalk-Ellerbroek LJ**, de Jong PA, van Montfrans JM, Lammers JW, Bloem AC, Hoepelman AI, Ellerbroek PM. CT screening for pulmonary pathology in common variable immunodeficiency disorders and the correlation with clinical and immunological parameters. *J Clin Immunol* 2014; **34**: 642-654 [PMID: 24952009 DOI: 10.1007/s10875-014-0068-6]

18 **van de Ven AA**, van Montfrans JM, Terheggen-Lagro SW, Beek FJ, Hoytema van Konijnenburg DP, Kessels OA, de Jong PA. A CT scan score for the assessment of lung disease in children with common variable immunodeficiency disorders. *Chest* 2010; **138**: 371-379 [PMID: 20299624 DOI: 10.1378/chest.09-2398]

19 **van de Ven AA**, de Jong PA, Hoytema van Konijnenburg DP, Kessels OA, Boes M, Sanders EA, Terheggen-Lagro SW, van Montfrans JM. Airway and interstitial lung disease are distinct entities in paediatric common variable immunodeficiency. *Clin Exp Immunol* 2011; **165**: 235-242 [PMID: 21635229 DOI: 10.1111/j.1365-2249.2011.04425.x]

20 **van Zeggeren L**, van de Ven AA, Terheggen-Lagro SW, Mets OM, Beek FJ, van Montfrans JM, de Jong PA. High-resolution computed tomography and pulmonary function in children with common variable immunodeficiency. *Eur Respir J* 2011; **38**: 1437-1443 [PMID: 21659412 DOI: 10.1183/09031936.00173410]

21 European Society for Immunodeficiencies Registry Working Party. Working definitions for clinical diagnosis of PID. Available from: http://esid.org/Working-Parties/Registry/Diagnosis-criteria

22 **Miller MR**, Hankinson J, Brusasco V, Burgos F, Casaburi R, Coates A, Crapo R, Enright P, van der Grinten CP, Gustafsson P. Standardisation of spirometry. *Eur Respir J* 2005; **26**: 319-338 [PMID: 16055882 DOI: 10.1183/09031936.05.00034805]

23 **Pellegrino R**, Viegi G, Brusasco V, Crapo RO, Burgos F, Casaburi R, Coates A, van der Grinten CP, Gustafsson P, Hankinson J. Interpretative strategies for lung function tests. *Eur Respir J* 2005; **26**: 948-968 [PMID: 16264058 DOI: 10.1183/09031936.05.00035205]

24 **Hansell DM**, Bankier AA, MacMahon H, McLoud TC, Müller NL, Remy J. Fleischner Society: glossary of terms for thoracic imaging. *Radiology* 2008; **246**: 697-722 [PMID: 18195376 DOI: 10.1148/radiol.2462070712]

25 **Tanaka N**, Kim JS, Bates CA, Brown KK, Cool CD, Newell JD, Lynch DA. Lung diseases in patients with common variable immunodeficiency: chest radiographic, and computed tomographic findings. *J Comput Assist Tomogr* 2006; **30**: 828-838 [PMID: 16954938 DOI: 10.1097/01.rct.0000228163.08968.26]

26 **Thickett KM**, Kumararatne DS, Banerjee AK, Dudley R, Stableforth DE. Common variable immune deficiency: respiratory manifestations, pulmonary function and high-resolution CT scan findings. *QJM* 2002; **95**: 655-662 [PMID: 12324637 DOI: 10.1093/qjmed/95.10.655]

27 **Martínez García MA**, de Rojas MD, Nauffal Manzur MD, Muñoz Pamplona MP, Compte Torrero L, Macián V, Perpiñá Tordera M. Respiratory disorders in common variable immunodeficiency. *Respir Med* 2001; **95**: 191-195 [PMID: 11266236 DOI: 10.1053/rmed.2000.1020]

28 **Aghamohammadi A**, Allahverdi A, Abolhassani H, Moazzami K, Alizadeh H, Gharagozlou M,

Kalantari N, Sajedi V, Shafiei A, Parvaneh N. Comparison of pulmonary diseases in common variable immunodeficiency and X-linked agammaglobulinaemia. *Respirology* 2010; **15**: 289-295 [PMID: 20051045 DOI: 10.1111/j.1440-1843.2009.01679.x]

29 **van de Ven AA**, van de Corput L, van Tilburg CM, Tesselaar K, van Gent R, Sanders EA, Boes M, Bloem AC, van Montfrans JM. Lymphocyte characteristics in children with common variable immunodeficiency. *Clin Immunol* 2010; **135**: 63-71 [PMID: 20006554 DOI: 10.1016/j.clim.2009.11.010]

30 **Sweinberg SK**, Wodell RA, Grodofsky MP, Greene JM, Conley ME. Retrospective analysis of the incidence of pulmonary disease in hypogammaglobulinemia. *J Allergy Clin Immunol* 1991; **88**: 96-104 [PMID: 2071789 DOI: 10.1016/0091-6749(91)90306-9]

31 **Berger M**, Geng B, Cameron DW, Murphy LM, Schulman ES. Primary immune deficiency diseases as unrecognized causes of chronic respiratory disease. *Respir Med* 2017; **132**: 181-188 [PMID: 29229095 DOI: 10.1016/j.rmed.2017.10.016]

32 **Miller WT Jr**, Panosian JS. Causes and imaging patterns of tree-in-bud opacities. *Chest* 2013; **144**: 1883-1892 [PMID: 23948769 DOI: 10.1378/chest.13-1270]

33 **Rossi SE**, Franquet T, Volpacchio M, Giménez A, Aguilar G. Tree-in-bud pattern at thin-section CT of the lungs: radiologic-pathologic overview. *Radiographics* 2005; **25**: 789-801 [PMID: 15888626 DOI: 10.1148/rg.253045115]

34 **Kainulainen L**, Nikoskelainen J, Vuorinen T, Tevola K, Liippo K, Ruuskanen O. Viruses and bacteria in bronchial samples from patients with primary hypogammaglobulinemia. *Am J Respir Crit Care Med* 1999; **159**: 1199-1204 [PMID: 10194166 DOI: 10.1164/ajrccm.159.4.9807067]

35 **Gosset N**, Bankier AA, Eisenberg RL. Tree-in-bud pattern. *AJR Am J Roentgenol* 2009; **193**: W472-W477 [PMID: 19933620 DOI: 10.2214/AJR.09.3401]

36 **Tashtoush B**, Okafor NC, Ramirez JF, Smolley L. Follicular Bronchiolitis: A Literature Review. *J Clin Diagn Res* 2015; **9**: OE01-OE05 [PMID: 26500941 DOI: 10.7860/JCDR/2015/13873.6496]

37 **Camarasa Escrig A**, Amat Humaran B, Sapia S, León Ramírez JM. Follicular bronchiolitis associated with common variable immunodeficiency. *Arch Bronconeumol* 2013; **49**: 166-168 [PMID: 22963957 DOI: 10.1016/j.arbres.2012.06.007]

38 **Bates CA**, Ellison MC, Lynch DA, Cool CD, Brown KK, Routes JM. Granulomatous-lymphocytic lung disease shortens survival in common variable immunodeficiency. *J Allergy Clin Immunol* 2004; **114**: 415-421 [PMID: 15316526 DOI: 10.1016/j.jaci.2004.05.057]

39 **Tashtoush B**, Memarpour R, Ramirez J, Bejarano P, Mehta J. Granulomatous-lymphocytic interstitial lung disease as the first manifestation of common variable immunodeficiency. *Clin Respir J* 2018; **12**: 337-343 [PMID: 27243233 DOI: 10.1111/crj.12511]

40 **Touw CM**, van de Ven AA, de Jong PA, Terheggen-Lagro S, Beek E, Sanders EA, van Montfrans JM. Detection of pulmonary complications in common variable immunodeficiency. *Pediatr Allergy Immunol* 2010; **21**: 793-805 [PMID: 19912551 DOI: 10.1111/j.1399-3038.2009.00963.x]

41 **Edgar JD**, Buckland M, Guzman D, Conlon NP, Knerr V, Bangs C, Reiser V, Panahloo Z, Workman S, Slatter M. The United Kingdom Primary Immune Deficiency (UKPID) Registry: report of the first 4 years' activity 2008-2012. *Clin Exp Immunol* 2014; **175**: 68-78 [PMID: 23841717 DOI: 10.1111/cei.12172]

P- Reviewer: Bazeed MF, Chow J, Gao BL, Lacalzada-Almeida J, Tang GH
S- Editor: Ji FF **L- Editor:** A **E- Editor:** Huang Y

Published By Baishideng Publishing Group Inc
7901 Stoneridge Drive, Suite 501, Pleasanton, CA 94588, USA
Telephone: +1-925-2238242
Fax: +1-925-2238243
E-mail: bpgoffice@wjgnet.com
Help Desk: https://www.f6publishing.com/helpdesk
https://www.wjgnet.com